Bioactive Materials 7 (2022) 227–241

Contents lists available at ScienceDirect

Bioactive Materials

journal homepage: www.sciencedirect.com/journal/bioactive-materials

High-throughput drug screening models of mature adipose tissues which replicate the physiology of patients' Body Mass Index (BMI)

Fiona Louis [a], Yoshihiro Sowa [c,**], Shiro Kitano [a,d], Michiya Matsusaki [a,b,*]

[a] Osaka University, Joint Research Laboratory (TOPPAN) for Advanced Cell Regulatory Chemistry, Graduate School of Engineering, 2-1 Yamadaoka, Suita Osaka, 565-0871, Japan
[b] Osaka University, Graduate School of Engineering, Department of Applied Chemistry, 2-1 Yamadaoka, Suita Osaka, 565-0871, Japan
[c] Kyoto Prefectural University of Medicine, Department of Plastic and Reconstructive Surgery, Graduate School of Medical Sciences, Kamigyo-ku Kajii-cho, Kawaramachi-Hirokoji, Kyoto, 602-8566, Japan
[d] TOPPAN PRINTING CO., LTD., Technical Research Institute, 4-2-3 Takanodaiminami, Sugito-machi, Saitama, 345-8508, Japan

ARTICLE INFO

Keywords:
Mature vascularized adipose tissue reconstruction
High-throughput drug-screening model
Obesity
BMI
Diabetes

ABSTRACT

Obesity is a complex and incompletely understood disease, but current drug screening strategies mostly rely on immature *in vitro* adipose models which cannot recapitulate it properly. To address this issue, we developed a statistically validated high-throughput screening model by seeding human mature adipocytes from patients, encapsulated in physiological collagen microfibers. These drop tissues ensured the maintenance of adipocyte viability and functionality for controlling glucose and fatty acids uptake, as well as glycerol release. As such, patients' BMI and insulin sensitivity displayed a strong inverse correlation: the healthy adipocytes were associated with the highest insulin-induced glucose uptake, while insulin resistance was confirmed in the underweight and severely obese adipocytes. Insulin sensitivity recovery was possible with two type 2 diabetes treatments, rosiglitazone and melatonin. Finally, the addition of blood vasculature to the model seemed to more accurately recapitulate the *in vivo* physiology, with particular respect to leptin secretion metabolism.

1. Introduction

The scale of the global obesity epidemic (globally, more than 650 million people [1]) requires an in-depth understanding of the mechanisms underlying this complex disease and the prevalence of its related conditions, such as type 2 diabetes (463 million [2]), or other comorbidities including cancers, sleep apnea, asthma, degenerative joint disease, hypertension, renal failure, stroke and cardiovascular disease [3,4]. While previously considered merely as energy storage, it is clear now that adipose tissue is a dynamic endocrine organ secreting many different bioactive factors necessary for insulin sensitivity, energy metabolism, immune responses and cardiovascular homeostasis [5] in addition to providing insulation and mechanical support for the body [6]. The regulation of this endocrine organ's secretions is complex and multifactorial, therefore there is as yet no cure for obesity. Pharmacological approaches have several unpredictable side effects while current healthcare policy is limited to the promotion of physical activity along with reduction of fats and sugars consumption.

A suitable *in vitro* model with physiological functionality has long been needed to further understand the mechanisms of human obesity. The translation from animal models is limited by their metabolic heterogeneity, especially between murine and human types [7–9], which slows down human drug development. To speed up the drug discovery process, high-throughput screening (HTS) is an important tool for screening large small-molecule libraries until identifying effective compounds [10]. Currently, the vast majority of HTS against obesity are conducted on cultured cells grown in two dimensions (2D) which does not represent the complex cell microenvironment of *in vivo* adipose tissue [11–14] and could contribute markedly to their drug discovery high failure rate with low clinical trials correlation [15,16]. 2D adipocytes cannot achieve their *in vivo* final spherical shape, optimized to maximize their lipid storage, leading to increased cytoskeletal stress and

Peer review under responsibility of KeAi Communications Co., Ltd.
* Corresponding author. Osaka, 565-0871, 2-1 Yamadaoka, Suita, Japan.
** Corresponding author. Kyoto, 602-8566, Kamigyo-ku Kajii-cho, Kawaramachi-Hirokoji, Japan.
E-mail addresses: f-louis@chem.eng.osaka-u.ac.jp (F. Louis), sowawan@koto.kpu-m.ac.jp (Y. Sowa), shiro.kitano@toppan.co.jp (S. Kitano), m-matsus@chem.eng.osaka-u.ac.jp (M. Matsusaki).

https://doi.org/10.1016/j.bioactmat.2021.05.020
Received 12 March 2021; Received in revised form 27 April 2021; Accepted 7 May 2021
Available online 30 May 2021

a lack of the close cell-cell and cell-extracellular matrix (ECM) signals necessary for the adipose tissue homeostasis. Therefore, 3D cell culture technologies which better represent the *in vivo* environment are of importance for time and cost saving in drug discovery [16,17], as well as for use as diagnostic tools. Most of the currently available 3D human *in vitro* adipose tissue models involve monocultures of differentiated bone marrow–derived mesenchymal stem cells, adipose tissue–derived mesenchymal stem cells (adipose-derived-stem cells, ADSC), or embryonic stem cells cultured with synthetic or natural polymeric matrices and scaffolds [18,19]. However, these models of differentiated adipocytes from mesenchymal stem cell progenitors are still in an immature state with a final low ratio of differentiated cells [20] and a lower basal adipose metabolism compared to the native mature adipocytes [21,22]. The best way to obtain a physiological adipose tissue model would be the direct use of primary mature adipocytes to get comparable identity and functions than native tissue [21,22]. But, as they possess a cytoplasm composed of 80–90% lipids, they are easily traumatized by mechanical forces during the adipose tissue isolation process, resulting in a high ratio of damaged cells. Also, their maintenance more than one week *in vitro* still remains a challenge [23,24], while being already terminally differentiated, they cannot proliferate. Therefore, only a few published models used mature adipocytes [22,25,26], with limited HTS application and none of them have considered the specific cell phenotype exhibited in the case of obesity or type 2 diabetes.

Indeed, the association between adipose tissue and the insulin resistance found in the type 2 diabetes has been widely reported [27], but only a few *in vitro* models mimic this physiological condition [28,29]. The current studies for diabetes therapeutics have either used a 2D environment, sometimes with non-human immortalized cell lines, differentiated in adipocyte monocultures [30], or a co-culture with macrophages or peripheral blood mononuclear cells [31–33]. However, these models still did not use physiological obese adipocytes to model diabetes-related cell responses, the key factor for accelerating the screening of drugs for insulin resistance-induced diabetes.

Another point that ultimately limits all of the current models in their ability to recapitulate structural and functional adipose tissue is their lack of blood vessels vasculature, which plays a critical role in its physiological functions, being one of the most vascularized tissues in the body [34]. The adipose blood vessel provides nutrients, oxygen, cells, and various soluble factors to maintain its tissue homeostasis while carrying out adipokine secretions. Inadequate vascularization leads to hypoxia, inflammation and necrosis [34]. This dense vascularization also allows adipocytes and endothelial cells to be in direct contact for their cellular crosstalk. Adipocytes can guide the endothelial cells migration and proliferation [35] by secreting both pro- and anti-angiogenic factors, while the vascular system supports adipocytes growth and function [34]. Existing studies have attempted to induce adipogenesis of ADSC along with vasculature establishment from endothelial cells [36–44], but a functional culture medium allowing differentiation of adipocytes up to a mature differentiated state with endothelial cells in co-culture still appears to be a major challenge.

To address all these needs, we recently developed collagen microfibers (CMF) from collagen type I, the most prevalent in adipose tissue, which improved the maintenance of mature adipocyte viability and function [45], while providing a physiological environment and biological signals for the cells. This microenvironment limits the shear stress (i.e. the frictional force that acts on cell surface) around the fragile mature adipocytes, allows the nutrient and oxygen diffusion and help to guide the endothelial cells vasculature construction through their integrin-induced adhesion on the fibers [35,39,46]. The importance of ADSC for the formation of endothelial tubular structures, in addition to mature adipocytes, was confirmed in our previous model [47], showing the development of an *in vitro* vascularized adipose tissue. The same method was thus used here but on a smaller scale, in 96-well plates, to fulfill the HTS application for obesity related drug screening, where adipocytes' insulin responses are dependent on the patient's BMI. This personalized patient-related model should allow the development of more accurate therapeutic approaches to mitigate the obesity epidemic and its adverse effects on health. To ensure it, the quality of the HTS assay was finally statistically analyzed with the current validated quality control metrics: Z′-factor, Signal-to-noise ratio (S/N), Signal-to-background ratio (S/B), coefficients of variation (CV), as well as the strictly standardized mean difference (SSMD) and its reciprocal, the coefficient of variation of difference (CVD).

2. Results

In a previous report, we described an innovative bio-fabrication method for the reconstruction of vascularized adipose tissues [47]. Adjusting this methodology, we focused here on the design of a smaller scale mature adipose tissue model suitable for the HTS of molecules against obesity in a mimicked physiological condition (Fig. 1).

2.1. Preliminary developments for a suitable mature adipocytes' viability maintenance in the adipose drop model

The first step was to assess the most suitable condition for the maintained viability of the fragile mature adipocytes. Human mature adipocytes isolated from abdominal adipose tissues, mixed with CMF and embedded in a fibrin gel were thus seeded in different conditions (Fig. 2a). The same condition used in the previous study (1.2%wt CMF [47]) with 3×10^6 mature adipocytes/mL (condition 2) was compared with a two-fold higher CMF concentration (condition 1, 2.4%wt CMF), a 50% cell concentration (1.5×10^6 mature adipocytes/mL, 1.2%wt CMF, condition 3) and a condition without any CMF (3×10^6 mature adipocytes/mL, condition 4). For all conditions, the culture medium volume was also compared, by seeding the same 2 μL drop tissue in either 96- or 48-well plates, containing 300 μL or 1.2 mL volume respectively (Fig. 2b). After one week, all conditions showed good maintenance of the mature adipocytes viability, from 87 to 97% of living cells, with a high reproducibility between the samples. From the 2 and 3 weeks results, two conditions (2 and 4) showed a tendency for a better maintained mature adipocytes viability, with respectively 74-86% and 79-97% of living cells, depending on the culture medium volume. While few differences were observed between the two culture medium volumes for the previous weeks of culture, after 3 weeks the 96-well plates appeared mostly with a higher viability so this was then chosen for all the experiments as it better fits the requirements of the HTS model. Even though condition 4 gave the best viability results (97 ± 1% for the 96-well plate), the observation of the mature adipocytes state revealed a high ratio of spindle and elongated structures similar to fibroblasts (Fig. 2c), which can come from dedifferentiated mature adipocytes, or a proliferation of the small amount of ADSC which can stayed attached to the mature adipocytes during the cell isolation (around 0.2–0.4% generally [19,48]). For condition 2, some mature adipocytes also dedifferentiated or died, but more could maintain their unilocular shape, with a smaller proliferation rate (Fig. 2c, white arrow). To optimize the culture condition, using the same mixture as condition 2 (3×10^6 mature adipocytes/mL with 1.2%wt CMF), several drop tissue volumes were compared (1, 2, 3 and 5 μL) (Fig. 2d), as well as the culture medium composition, comparing the classic DMEM medium with the Human Adipocyte Differentiation Medium (containing indomethacin, 3-isobutyl-1-methylxanthine, dexamethasone and insulin). It was noted that the adipogenesis growth factors hindered the mature adipocytes viability after one week of culture, while in the classic DMEM medium, all drops volumes showed good viability. The difference was emphasized after 2 weeks of culture, the 2 μL drops showing a higher ratio of living mature adipocytes compared to the other volumes (Fig. 2e). In particular, in the 5 μL drop condition, several mature adipocytes were found dedifferentiated with an elongated cell shape. The 2 μL drop volume was thus chosen for the later experiments, displaying a high viability of 99 ± 0.1% and 77 ± 5% after 1 and 2 weeks respectively (Fig. 2f). In this

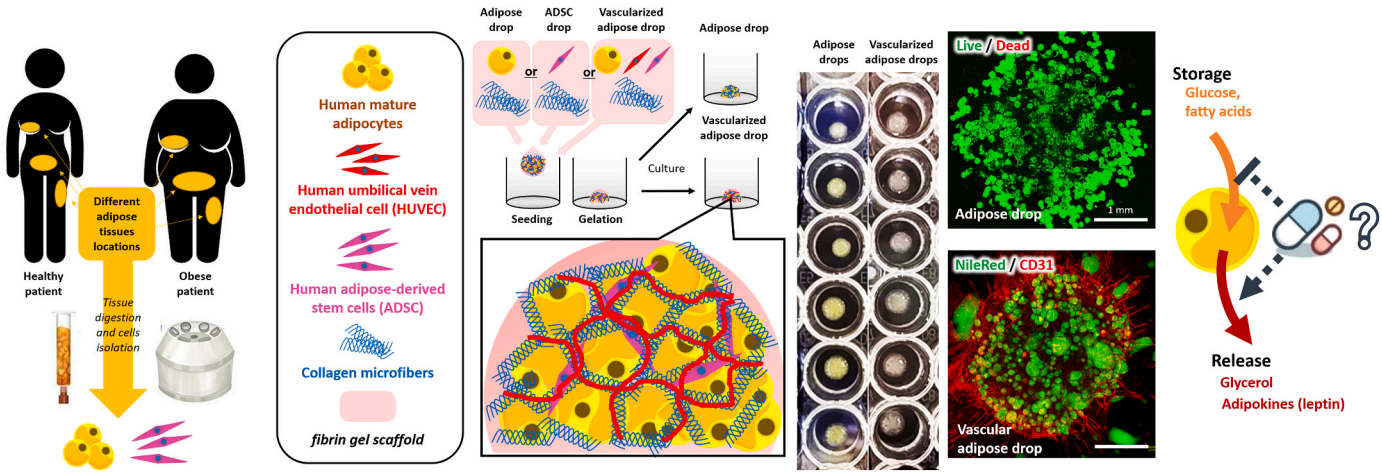

Fig. 1. High-throughput screening adipose drop model methods. Using human adipose tissues from different types of patients and different tissue locations, mature adipocytes and adipose-derived stem cells (ADSC) were isolated after tissue digestion. Adding human umbilical vein endothelial cell (HUVEC) and collagen microfibers type I, embedded in a fibrin gel, the mixture was seeded inside 96-well plates to make the adipose drop model. ADSC drops were also fabricated using only ADSC and non-vascularized drops using only mature adipocytes. These three models were analyzed by monitoring their viability through the culture, as well as their functionality by glucose or fatty acids uptake measurements and glycerol or leptin release, depending on inhibitor or inducer treatments, as well as known type 2 diabetes drugs.

condition, all adipocytes could maintain their unilocular shape, as confirmed by Nile Red staining shown in Fig. 2g. While the previous drop tissues were seeded using mature adipocytes isolated from abdominal adipose tissue, a comparison was made using other tissue locations. Mature adipocytes from either thigh adipose tissue (extracted after liposuction) or breast adipose tissue both showed a high viability in this model, 97 ± 0.4% and 98 ± 0.7% respectively, and could therefore be used for specific location-related studies.

2.2. Functionality maintenance of mature adipocytes in the adipose drop model

The next step was to monitor the maintenance of the mature adipocyte's functions in the drop tissues. Among the major adipocyte functions, the first is to store glucose and fatty acids in their lipid vesicles and then to release them in the form of glycerol to address body energy needs. Insulin secreted by the pancreas is the physiological inducer of this lipid storage, and it is released in response to elevated glucose levels in the blood. To visualize and quantify the glucose and fatty acids uptake in the *in vitro* mature adipocytes in an HTS format (96 well plates, Fig. 3a), the fluorescent analogues 2-NBDG (Fig. 3b) and BODIPY™ 500/510 (Fig. 3c) for glucose and fatty acids respectively, were used. Insulin was thus added to the culture medium after a glucose starvation of the adipocytes, then glucose and fatty acids uptake were monitored (Fig. 3b and c). The adipocytes of the drop tissues showed significantly induced storage of glucose and fatty acids from 5 to 135 min of insulin treatment. This adipose function being validated, molecules allowing the blockage of these two uptakes were then screened, against obesity. In the case of a high fed state, insulin binds to its receptors on the adipocytes and causes the translocation of glucose transporter 4 (Glut-4) from the cytosol to the cell surface, which then enables the effective glucose influx into the adipocytes [49]. Insulin-stimulated Glut-4 is the predominant glucose transporter type in adipocytes, but another glucose transporter type, Glut-1, is also constitutively present at their cell membranes [50]. Specific inhibitors of glucose transporters 1 and 4 were thus chosen (apigenin [51] and cytochalasin B [52] respectively). Fig. 3d shows the different combination effects of the two inhibitors, with or without insulin, on the glucose uptake. Only the condition with inhibitions of both Glut-1 and Glut-4 transporters was found to significantly reduce glucose uptake in the mature adipocytes compared to the control condition (apigenin effect only is shown in Supplementary Figure 2).

Both glucose and fatty acids uptake inhibition and induction can actually be assessed (Fig. 3e). TNFα [53] which can act on the translocation of the fatty acids transporters and reduce the activity of the lipoprotein lipase was used for the fatty acids uptake inhibition. In these mature adipocyte drop tissues, significant inhibitions (−86% and −173% for glucose and fatty acids uptake respectively compared to the control) or inductions (+83% and +538% for glucose and fatty acids uptake respectively compared to the control) of the uptakes were confirmed after 30 min of treatment.

Next, the glycerol release induction, which is also a way to fight obesity, was assessed by using two different classic inducers (Fig. 3f): isoproterenol and forskolin [54]. Isoproterenol, currently a non-FDA approved β adrenoreceptor agonist, because of its several side-effects like cardiac toxicity, and forskolin, also a non-FDA approved medicine from the mint family, inducing low blood pressure (hypotension), both significantly induced glycerol release from adipocytes in the drop tissues model in a dose-dependent manner.

While Fig. 3e highlighted the glucose uptake results of several adipose drop tissues seeded using mature adipocytes isolated from one patient, it was also possible to show the tendency for the insulin-induced and cytochalasin/apigenin-inhibited glucose uptake through several patients' adipose tissues. Fig. 3g shows the average of 18 different adipose tissues results from 18 different patients after 7 days of *in vitro* culture. Although many mature adipocytes types were observed in these 18 patients, with different ages and different body mass index (BMI) (from 14.2 to 36.6), the mean results displayed a significant induction of glucose uptake (from +26% up to 37%, compared to the control, Fig. 3g) after 5, 30 and 60 min of insulin treatment and a significant inhibition (−16%, compared to the control) after 30 min of inhibitor treatment. In comparison, after 14 days of *in vitro* culture, no significant differences were found between the control condition and the induced or inhibited ones (from +13% to +16% and maximum −8%, for an average of 9 different patients, Fig. 3h). This was also the case for the fatty acids uptake measurements of 13 different patients (Supplementary Figure 3). This reduced mature adipocyte sensitivity can be a bias from the *in vitro* culture condition where culturing the mature adipocytes in DMEM high glucose medium for 2 weeks might induce their insulin resistance [55, 56]. This model still allows to get, after 7 days of culture, a reliable tool for assessing drugs acting on the glucose/fatty acids uptakes or the glycerol release in the obesity fighting strategy.

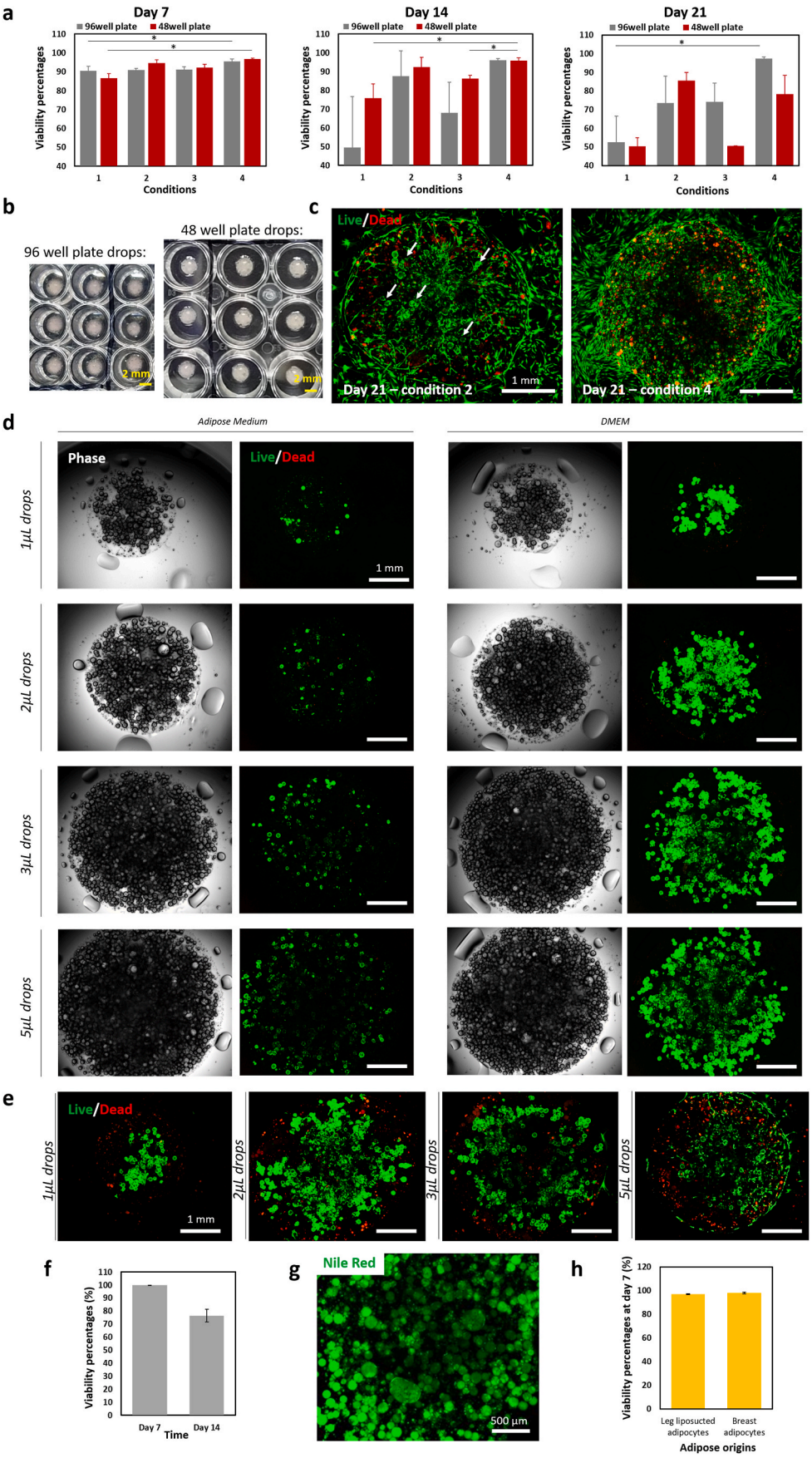

Fig. 2. Preliminary developments for a suitable mature adipocytes maintenance in the adipose drop model. (a) Live/Dead quantifications of mature adipocytes viability from abdominal adipose tissue, according to the drop compositions (condition 1: 3×10^6 mature adipocytes/mL + 2.4% wt CMF, condition 2: 3×10^6 mature adipocytes/mL + 1.2% wt CMF, condition 3: 1.5×10^6 mature adipocytes/mL + 1.2% wt CMF, condition 4: 3×10^6 mature adipocytes/mL + 0% wt CMF) and the culture medium volumes (96-well: 300 µL, 48-well: 1.2 mL). (b) Pictures of the drops after gelation. (c) Representative Live/Dead projection images of mature adipocytes after 3 weeks for conditions 2 and 4. (d) Representative Live/Dead projection images of mature adipocytes after 1 week in different drop tissue volumes and different culture medium. (e) Representative Live/Dead projection images of mature adipocytes after 2 weeks in different drop tissue volumes in DMEM. (f) Quantification of the viability of the mature adipocytes in the 2 µL drop tissue model after 1 and 2 weeks of culture in DMEM. (g) Nile Red lipids staining of representative 2 µL drop tissue after 1 week of culture. (h) Quantification of the viability of the mature adipocytes from two other adipose tissue locations (thigh adipose tissue after liposuction and breast adipose tissue) after 1 week of culture in 2 µL drops in DMEM. All graphs show results as means ± s.d. of experiments performed on n = 3-6 drops per condition.

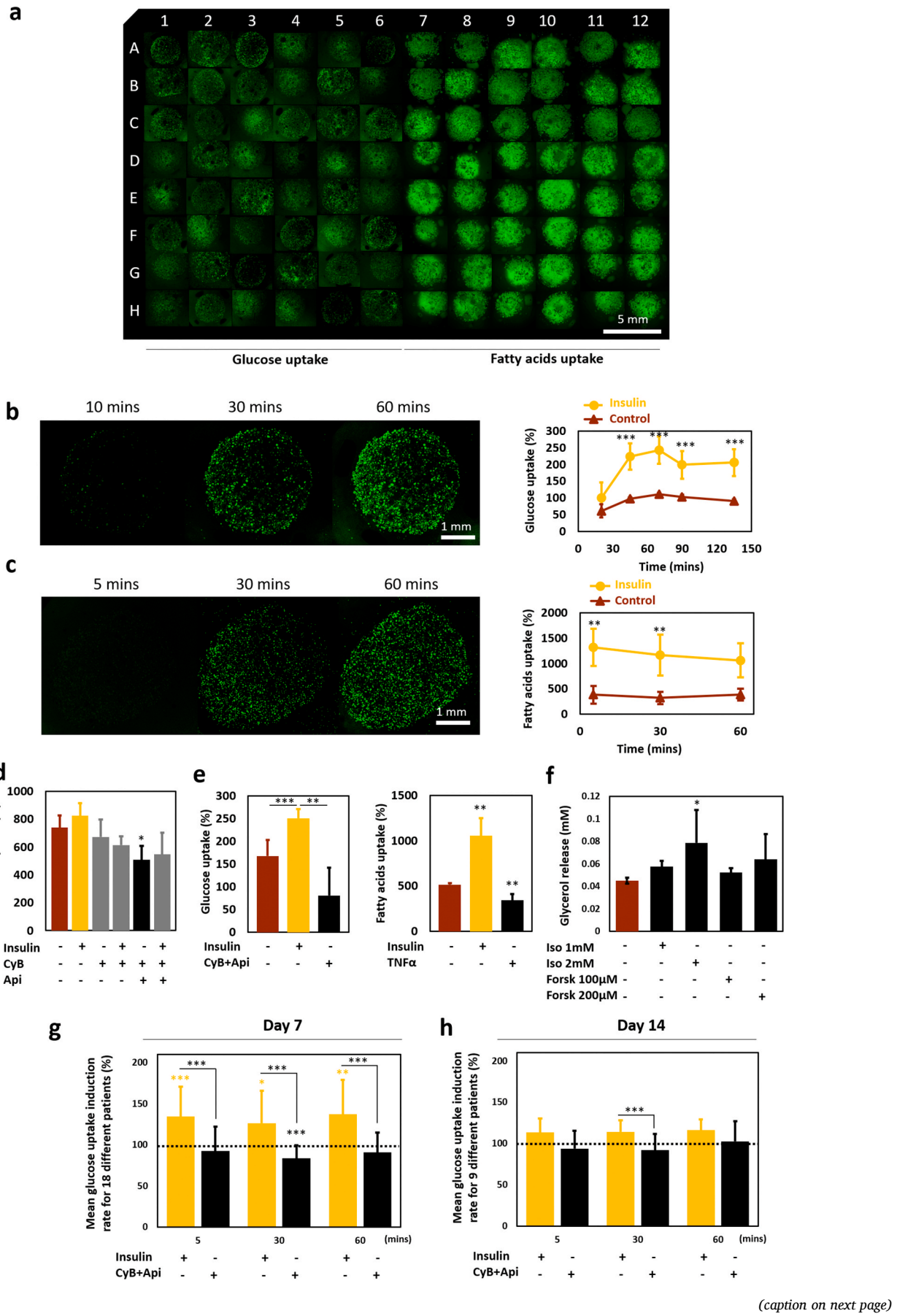

(caption on next page)

Fig. 3. Functionality assessment of mature adipocytes in the adipose drops model. (a) Example of glucose and fatty acids uptake measurements on a full 96-well plate at day 7 of culture. (b) Representative images of the 2-NBDG (2-(N-(7-Nitrobenz-2-oxa-1,3-diazol-4-yl)Amino)-2-Deoxyglucose) fluorescent glucose analogue uptake monitored inside the mature adipocytes cultured in the adipose drop model. Quantification of the 2-NBDG uptake through the time and after insulin treatment. (c) Representative image of the BODIPY™ 500/510 fluorescent fatty acids analogue monitored inside the mature adipocytes cultured in the adipose drop model. Quantification of the BODIPY™ 500/510 uptake through the culture time and after insulin treatment. (d) Measurements of glucose uptake after several induction or inhibition treatments during 30 min (Api: apigenin which blocks glucose transporter 1, CyB: cytochalasin B which blocks glucose transporter 4) in mature adipocytes isolated from one donor adipose tissue. (e) Glucose and fatty acid uptake inductions and inhibitions after 30 min of treatments in mature adipocytes isolated from one donor adipose tissue. (f) Glycerol release measurements from mature adipocytes after glycerol release inducer treatments during 60 min, mature adipocytes were isolated from 3 different donors. (g) Summarized data of glucose uptake inductions and inhibitions for 18 different adipose tissue donors after 7 days of culture. (h) Summarized data of glucose uptake inductions and inhibitions for 9 different adipose tissue donors after 14 days of culture. All graphs show results as means ± s.d. of experiments performed on n = 5-8 drops per condition per donor.

2.3. Functionality assessment of the adipogenesis ADSC drop model

An adipogenesis drug model was developed in parallel, using human ADSC differentiating in mature adipocytes, which allowed the drug screening of compounds acting specifically on the adipogenesis to slow down the growth of adipocytes and thus the lipid storage. The glucose uptake was compared in these ADSC drops tissues with the 2D classic culture after 2 weeks of adipogenic differentiation. Adipogenesis occurred faster in the drop tissues than in 2D, as already reported in a previous model in transwells with mouse adipocytes [45], and as seen in particular on the fatty acids uptake pictures (Fig. 4a) where several lipid vesicles were observed in the 3D condition, in almost all cells, compared to 2D which displayed many undifferentiated cells. However, the glucose and fatty acids uptake induction and inhibition comparisons did not show any significant differences between 2D and 3D, confirming the fact that mature adipocytes are more functional than differentiated ones, even using a 3D model, for assessing drugs acting on the glucose/fatty acids uptake. Only insulin showed a tendency to induce both uptakes. A more suitable way could be to act on the adipogenesis during the adipocyte differentiation and retinoic acid, a common inhibitor, was used for this purpose. Retinoic acid, a derivative of vitamin A, comes from the carotenoid's family. It plays major roles in adipogenesis maturation inhibition by enhancing the pre-adipocyte gene expression and inhibiting C/EBPβ-mediated transcription. Its inhibition effect was assessed in the ADSC differentiated model. It was found that 3D ADSC adipose drop tissues showed a better inhibitory response that was

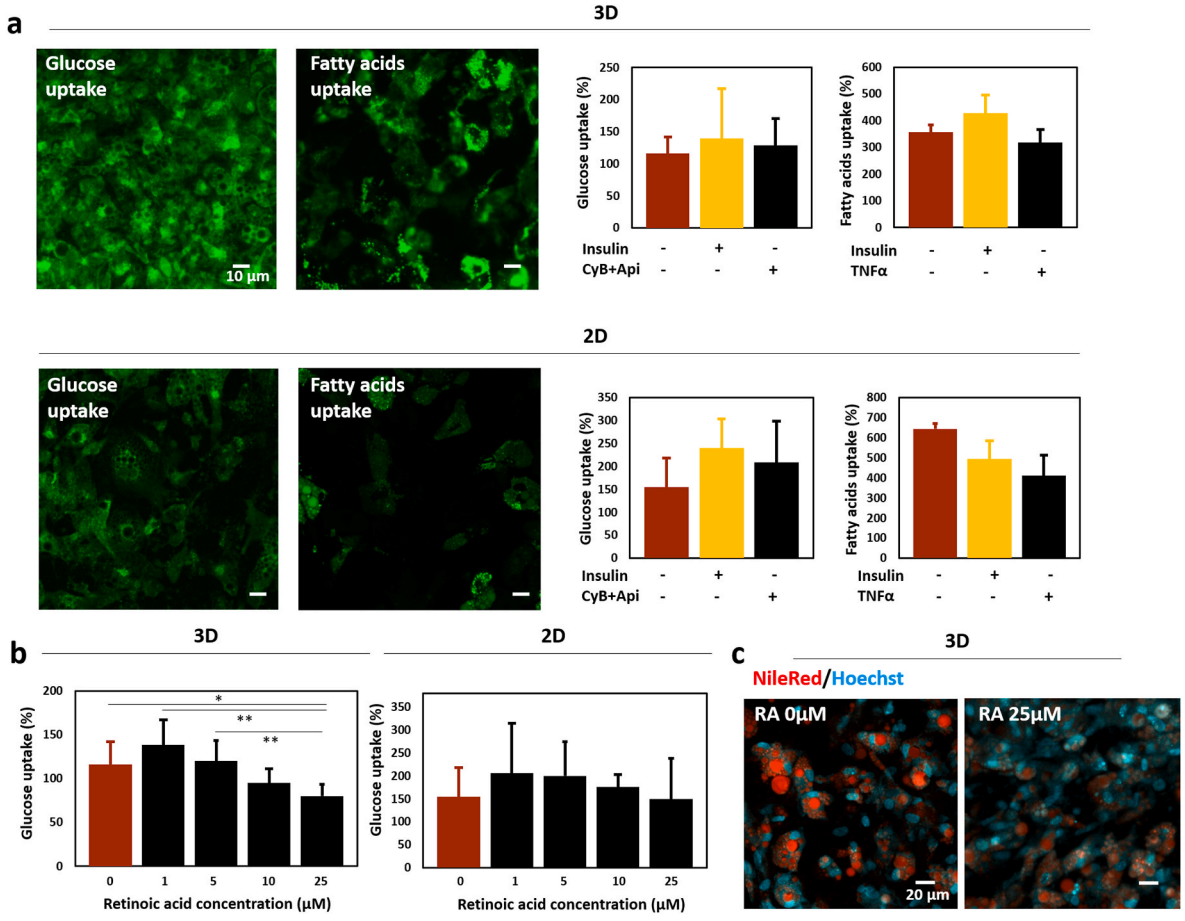

Fig. 4. Functionality assessment of the adipogenesis ADSC drop model. (a) Representative projection images of the ADSC drop model assessing the adipogenesis after 2 weeks of adipogenic differentiation, compared to the 2D classic condition. Glucose and fatty acids uptake measurements after 60 min of treatments using an inducer (insulin) and inhibitors (Api: apigenin, CyB: cytochalasin B, TNF-alpha) on the 2 weeks differentiated model in 2D or 3D (drops) condition. (b) 60 min duration glucose uptake measurements after 2 weeks of adipogenic differentiation of the ADSC drop model, compared to the 2D condition, using different concentrations of retinoic acid as an inhibitor during the adipogenesis. (c) Representative Nile Red (lipids) and Hoechst (nuclei) staining projection images of differentiating adipocytes in the ADSC drop model with or without retinoic acid (RA) treatment for 2 weeks. The graphs show results as means ± s.d. of experiments performed on n = 6-8 drops per condition.

significantly dependent on retinoic acid concentrations, compared to the 2D model (Fig. 4b), as confirmed by the smaller lipid vesicles observed after retinoic acid treatment (Fig. 4c). This can therefore be considered as a definitive model for investigating drugs acting specifically on adipogenesis inhibition against obesity.

2.4. Patients' BMI dependent glucose uptake sensitivity against insulin and insulin sensitivity recovery drug assays

BMI calculation allows the determination of the healthy state of patients and thus of their adipocyte function (see Fig. 5a for the ranges). Recently, the relationship between BMI and percentage of body fat or body fat distribution has been recognized as differing between ethnic populations and that the established World Health Organization (WHO) criteria for classifying obesity in adult Caucasians is not appropriate for Asian populations [57]. Japanese people indeed have lower BMIs at a given body fat and are more likely to develop complications such as impaired glucose tolerance, dyslipidemia and hypertension after exceeding BMI 25, while these happen at a higher BMI in Caucasian populations [58]. Therefore, lower BMIs in Asian populations need to be monitored more closely to prevent diabetes and related complications. As the study here was performed using only human adipose tissues from Japanese women, the specific Asian BMI classification was thus chosen, stipulating that overweight is specified for a BMI between 23.0 and 24.99, obesity for a BMI between 25.0 and 29.99, and severe obesity for a BMI over 30.0 [57].

Insulin sensitivity is closely linked to the BMI of each patient. Insulin resistance occurs when adipocytes start ignoring the signal that the insulin is sending out, even when the pancreas synthesizes more insulin to force adipocyte glucose uptake to reduce the glycemic level [59]. Obese patients usually show a lower insulin-induced glucose uptake due to the constantly excessive glucose level in their blood which leads to insulin resistance. The same is found in underweight patients, for opposite reasons [60]. This insulin resistance was found in our model when glucose uptake ability was plotted against the patients' BMI (Fig. 5a), confirming the increase of insulin resistance linked to the increase in the patients' BMI. An insulin sensitivity of around 1 represents insulin resistance, with no difference in glucose uptake when insulin is added. It was particularly found in the obese ($25.0 < BMI < 29.99$) and severely obese patients ($30.0 < BMI$). When the means for patients in the same BMI ranges were calculated, this BMI-dependent reduction of the insulin sensitivity trend was again confirmed (Fig. 5b).

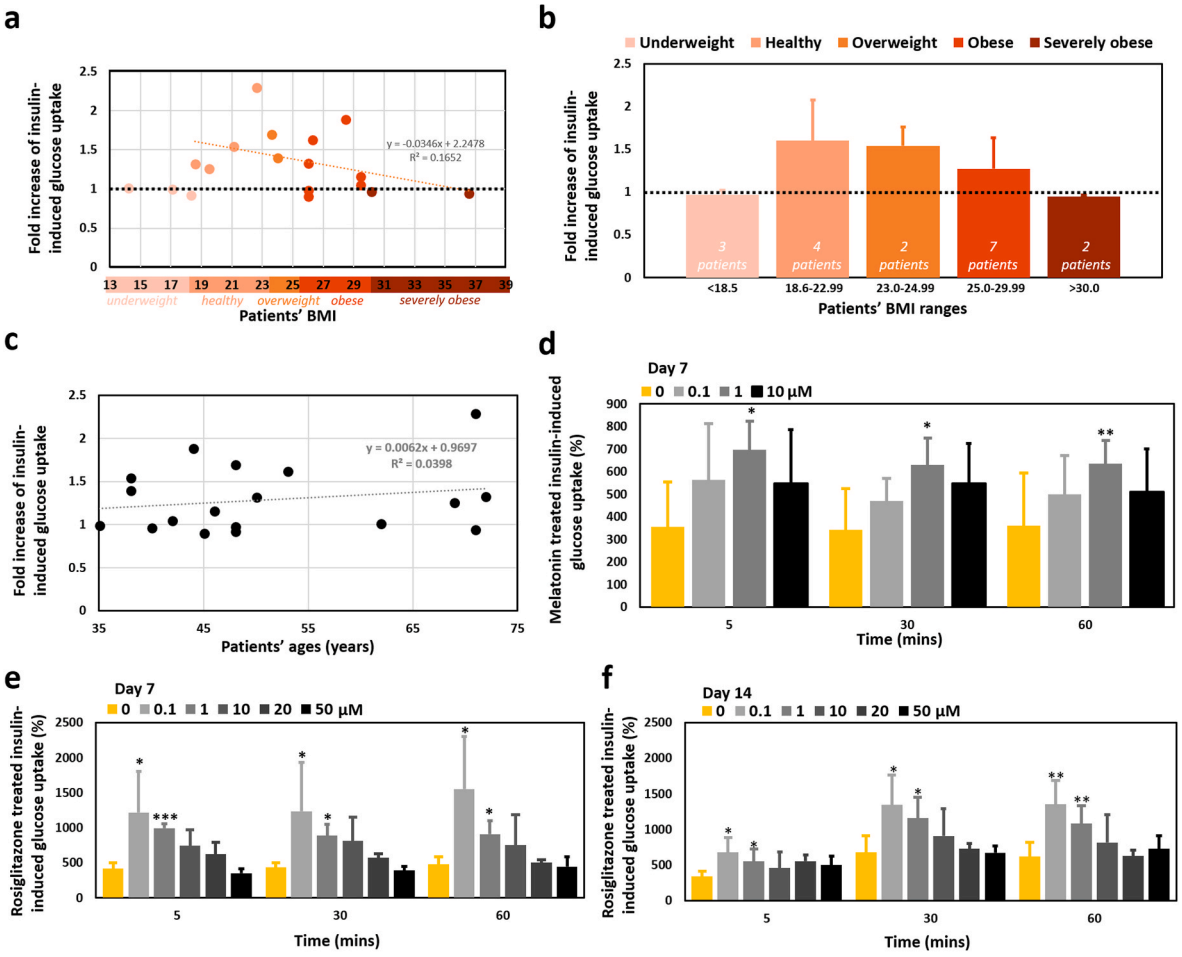

Fig. 5. Patients' BMI dependent glucose uptake sensitivity against insulin treatment and insulin sensitivity recovery drug assays. (a) Trend line of insulin sensitivity by glucose uptake, according to the patients' BMI after 30 min of treatment, for 18 different patients' mature adipocytes. (b) Histogram representation of the BMI-dependent insulin sensitivity for the 18 different patients. (c) Trend line of insulin sensitivity by glucose uptake, according to the patients' age after 30 min of treatment, for 18 different patients' mature adipocytes. (d) Concentration-dependent melatonin effect after 16 h of treatment on the 7 days cultured adipose drops model. The results represent the averages of 3 different donors (BMI 24.01, 26.3 and 23.6). (e) Concentration-dependent rosiglitazone effect after 16 h of treatment on the 7 days cultured adipose drops model. The results represent the averages of 3 different donors (BMI 24.01, 26.3 and 23.6). (f) Concentration-dependent rosiglitazone effect after 16 h of treatment on the 14 days cultured adipose drops model. The results are for two different donors (BMI 18.3 and 24.01). All graphs show results as means ± s.d. of experiments performed on n = 6-8 drops per condition per donor. Colored asterisks are compared to the control condition at each time.

On the other hand, the patient's age, which can also be associated with a lower insulin sensitivity, did not specifically show any tendency. For instance, two 71-year-old patients displayed very different insulin sensitivities, which more likely arose from their BMI difference (22.6 and 26) (Fig. 5c). As this insulin resistance has a key role in the development of type 2 diabetes, another important drug screening to perform is the recovery of insulin sensitivity in patients. Two treatments were then tested on the mature adipocytes model. The first one is an FDA-approved drug, currently used for type 2 diabetes patients [61], rosiglitazone, a PPARγ agonist which can improve the insulin resistance in human and murine adipose tissue [62]. The second one is melatonin, a non-FDA approved drug for type 2 diabetes which is a natural hormone secreted in the human body to maintain the wake-sleep cycles ("biological clock"). As short or poor quality sleep are associated with increased risk of obesity, this drug can help some patients to recover their insulin sensitivity [63]. The treatments using these two drugs in several concentrations were thus performed on the adipose drop tissues before measuring the insulin-induced glucose uptake. Both melatonin and rosiglitazone showed significant dose-dependent improvements in insulin sensitivity. The best induction was at 1 μM for melatonin (Fig. 5d) and at 0.1 μM for rosiglitazone (Fig. 5e), showing increased glucose uptakes in response to insulin, while the higher concentrations displayed saturated effects. This induced insulin sensitivity was even confirmed on 2-week cultured samples for the rosiglitazone treatment (Fig. 5f), even though it was assumed that culturing the mature adipocytes for 2 weeks in DMEM high glucose medium may have induced their insulin resistance (Fig. 3h). On the other hand, melatonin did not induce the recovery of insulin sensitivity after 2 weeks of culture (Supplementary Figure 4). Also, while the previous rosiglitazone and melatonin induction effect was observed in overweight and obese patients' mature adipocytes (BMIs of 23.6, 24.01 and 26.3), the recovery of insulin sensitivity was however not found anymore when seeding underweight (BMI of 17.1) and severely obese patients' mature adipocytes (BMI of 30.2) (Supplementary Figure 5).

These last data reinforce the limitations of existing drug screening methods. On the other hand, our novel approach shows promise as a good high-throughput screening model for specifically modeling patients' BMI differences in order to find suitable obesity or diabetes drugs.

2.5. Functionality assessment of the vascularized adipose drop model

Finally, non-vascularized adipose drop tissues were compared to vascularized adipose drop tissues. *In vivo*, blood vessels are of key importance for bringing glucose/fatty acids to the adipocytes and for the transportation of released glycerol and fatty acids. Similar drop tissues were seeded, containing ADSC and HUVEC in addition to the mature adipocytes in 2 μL volume and were cultured in endothelial medium with insulin to maintain the mature adipocytes (Fig. 6a). A dense blood vessels vasculature was observed surrounding the unilocular maintained mature adipocytes in the drops (Fig. 6b and c) in a similar way to *in vivo* highly vascularized adipose tissue.

To further compare with the *in vivo* adipose tissue characteristics, the adipose ECM was also assessed. While collagen type I, contributing considerably to the non-cell mass of the adipose tissue, was already added by the CMF content, the other components surrounding the mature adipocytes in the basal lamina, testifying their mature phenotype compared to preadipocytes [64], are known to be laminin and collagen type IV. These two components are produced by the adipocytes themselves and also the other cells of the stromal vascular fraction: the preadipocytes, the capillary endothelial cells and the ADSC [64,65]. Laminin forms a network with type IV collagen, promoting the endothelial cells attachment and migration [66]. In the adipose drop tissues, both network of collagen type IV and laminin were well observed in the vascularized condition (Fig. 6d), with the same pattern than *in vivo*, around the blood vessels and also slightly surrounding the mature adipocytes, but in a much lesser extent for the monoculture adipose drops, testifying the importance of the capillary network.

Concerning the lipid content, the vascularized adipose drop tissues were compared to the *in vivo* ones, showing non-significant differences when normalized by either the DNA content or the tissue weights (Supplementary Fig. 1a and b). The DNA amount was also used for comparing the total cellular content of both tissues and was found non-significantly different for their DNA amount/tissue weight (Supplementary Figure 1c). These two assessments reinforced the *in vivo* similarity of the model.

Aditionally, Live/Dead assay was performed after one week of culture displaying a high viability of the cells, but it was difficult to assess the specific viability of the mature adipocytes alone in this co-culture of three types of cells (Fig. 6e). The comparison of the glucose uptake assays were also evaluated between the adipose drops and the vascularized ones, and the results showed that the added vascularization allowed a significantly faster insulin-induced glucose uptake in the tissues (+383%, Fig. 6f) in 4 different patients' mature adipocytes. However, when considering the average of 11 different patients, this higher induction was mitigated, probably due to the wide range of BMIs (Supplementary Figure 3a).

Leptin hormone secretion was then measured during the culture time in the vascularized adipose drops and compared to the monoculture ones. Leptin is the satiety hormone secreted by the adipose tissue. A significantly better maintenance of leptin secretion was found in the vascularized adipose drops (21- and 18-fold increases at days 7 and 14 respectively, Fig. 6g), whereas a time-dependent decreased secretion was observed in the monoculture drops. This hormone shows dysregulation in cases of obesity where its level decreases while BMI increases, implying less satiety and a higher food intake compared to healthy people [67]. In our model, a strong inverse correlation between the leptin secretion levels and the patients' BMI was found, but only in the vascularized adipose drop tissues (Fig. 6h), which confirms the possible higher physiological behavior of adipocytes in this model. Leptin secretion is also supposed to increase with aging, when the redistribution of adipose tissue from subcutaneous to visceral observed during middle and old age contributes to an increase in circulating leptin [68]. This increasing tendency might also appear better modeled in the vascularized adipose drops (Supplementary Figure 6), which seems to recapitulate in a more similar way the *in vivo* adipose tissue metabolism.

2.6. Statistical validation of the HTS model

While this model of high throughput formats for adipose-targeting drug screening seemed to provide a robust model, the only way to fully validate it for HTS assays applications is to investigate the HTS specific assay metrics playing the critical gatekeeping role.

The current universal requirement is estimated by the calculation of the Z′-factor, initially introduced by Zhang et al. [69], to measure the separation between "positive control" wells and "negative control" wells, as observed in Fig. 7a and b in the case of the glucose and fatty acids uptakes for 96 monoculture mature adipose drop tissues of a full plate, at day 0 of culture.

The cut off criterions are as follow [69]: Z′-factor = 1 is considered as the hypothetically "ideal assay", $1 > Z'\text{-factor} \geq 0.5$ for "excellent assay", $0.5 > Z'\text{-factor} > 0$ for "doable assay", Z′-factor = 0 for "yes/no type assay" and $Z'\text{-factor} < 0$ for "screening essentially impossible." Using this Z′-factor-based criterion, it appeared that both glucose and fatty acids uptake measurements can be considered as excellent HTS assays, the separation between the positive and negative controls being clearly observed. By comparing the Signal-to-Noise (S/N) and Signal-to-Background (S/B) values, the fatty acids uptake measurement was found as slightly more reliable than the glucose uptake one, having higher values.

As the use of the Z′-factor, S/N and S/B alone can be unclear to conclude, the coefficient of variation (CV), the strictly standardized mean difference (SSMD) and the coefficient of variation of difference

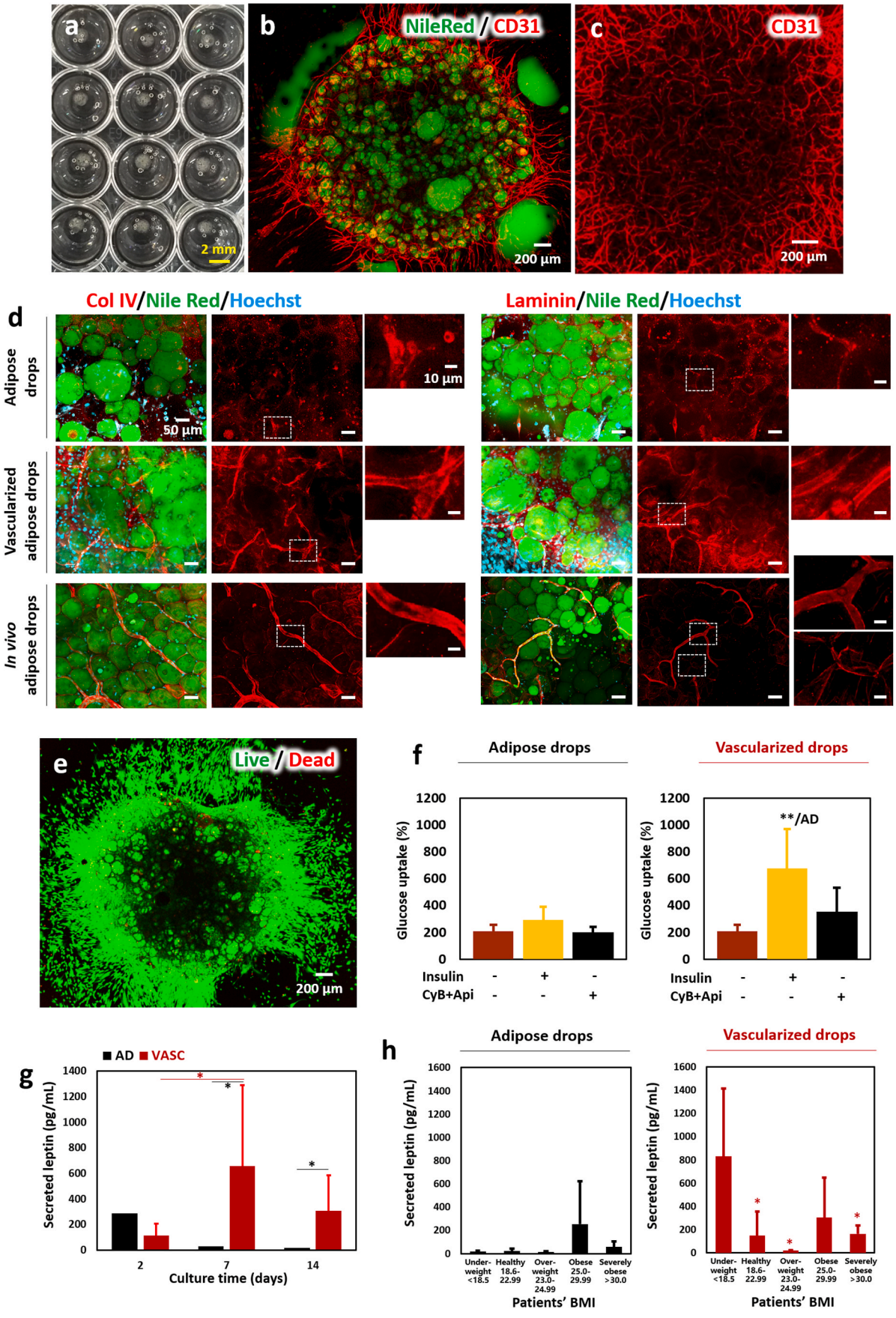

(caption on next page)

Fig. 6. Functionality assessment of the vascularized adipose drop model. (a) Picture of the vascularized adipose drop model in the 96-well plate after gelation. (b) Representative Nile Red (lipids) and CD31 (blood vessels) projection staining images after 1 week of culture in the vascularized adipose drop model. (c) Representative CD31 projection immunostaining image after RapidClear treatment for easier observation of the thickest part of the drop tissue. (d) Representative Collagen type IV, Laminin, Nile Red and CD31 projection staining images after 1 week of culture in the adipose drop models, compared to *in vivo* adipose tissues. (e) Representative Live/Dead projection images of the vascularized adipose drop model after 1 week of culture. (f) Glucose uptake measurement after insulin or inhibitors (Api: apigenin, CyB: cytochalasin B) treatment in the adipose and the vascularized adipose drop models, mean results of 4 different patients' mature adipocytes (BMI of 19.5, 23.6, 26.3 and 28.5). (g) Leptin secretion measurement in the supernatant of the adipose (AD) and the vascularized adipose (VASC) drop models after 2, 7 and 14 days of culture on 10 different patients' mature adipocytes. (h) Leptin secretion profiles according to the BMI ranges of the patients whose adipose tissues were isolated. Significant differences were compared to the underweight range. The graphs show results as means ± s.d. of experiments performed on n = 6-8 drops per condition per donor.

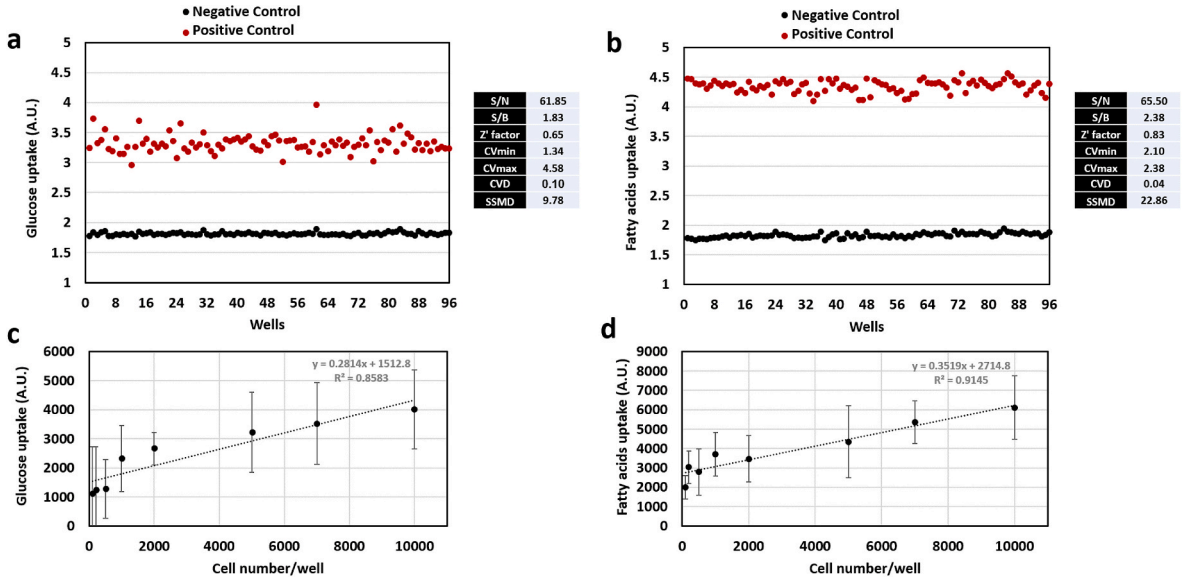

Fig. 7. Statistical validation of the HTS model. (a–b) Assay data of 96 well plates full of tissues for glucose and fatty acids uptakes fluorescence measurement of the positive and negative controls, in log-normalization. Tables of the S/N, S/B, Z' factor, CV_{min}, CV_{max}, CVD and SSMD values. (c–d) Relationship between the number of cells seeded per drop tissue and the fluorescence intensity during the glucose and fatty acids uptakes assays, with the linear regression correlation assessed by the slope equation and its R^2. The graphs show results as means ± s.d. of experiments performed on n = 8 drops per cell number.

(CVD) were also calculated. Measuring the CV across the whole plate ensures that the tissues seeding and the fluorescence reading were correctly functioning, and can reliably estimate the potential effects of the screened compounds. Generally, a distribution with a CV < 10% is considered of low-variance, while a CV > 10% is of high-variance [70,71]. For both glucose and fatty uptake measurements here, the signals had CV_{max} and CV_{min} in the range of 0–10%, testifying the high degree of reproducibility, even though the tissues seeding was performed manually here, the fatty acids uptake appearing again as more reliable.

Like Z'-factor, SSMD and CVD capture the variabilities in both compared populations, but are said to have a clear probability interpretation and a solid statistical basis [72]. Therefore, the larger the SSMD between two populations, the greater the differentiation between the two populations will be possible. For the CVD, it will be the opposite, the larger the CVD between two populations, the less the obtained differentiation. Thus, a SSMD ≥3 indicates that the size of the mean difference is at least three times that of the SD of the difference, and this threshold criterion can be considered [72]. In this study, again both glucose and fatty acids uptakes measurement had a SSMD ≥3 and a CVD close to 0, showing in a fairly clear way that the positive control was well differentiated from the negative control.

Finally, Fig. 7c and d illustrates the relationship between the cell number in the adipose drop tissues and the fluorescence intensity determined by the study assay method in the case of the glucose or the fatty acids uptakes measurements. A well-correlated linear relationship (R^2 = 0.8583 and R^2 = 0.9145, respectively for both assays) was assessed, following the increase of the cell number per tissue, which validates the relevance of using these assays for the adipose-targeting HTS drug screening.

3. Discussion

Whether vascularized or unvascularized, this HTS adipose drop tissue model shows clear potential for specific modeling of the adipose tissue in patients with different BMIs, thus addressing the complexities of obesity and its related diseases. The great challenge in this study was to deal with the large range of patients' BMI, leading to large error bars during the analysis, but which finally gave significant tendencies. This model appears to be a much better method than 2D classic cultures, also concerning the handling of the *in vitro* culture, as in a 2D monolayer the maturing adipocytes easily detach due to their lipid vesicles. This makes the assays difficult as the methods usually include several washing steps.

The added vascularization in the adipose drop model did provide a higher maintenance of the mature adipocytes metabolism, as illustrated in particular by the leptin secretion, however it was not always the case for the glucose and fatty acids uptake. This might also be explained by the insulin added in the endothelial culture medium to maintain the mature adipocytes, which could lead to a possible beginning of insulin resistance. Further studies are needed to more fully understand these data and thus the complexity of adipose tissue homeostasis.

Concerning leptin metabolism, its implication has already been reported in descriptions of the cross-talk between blood vessels vasculature and adipocytes. During preadipocytes differentiation for instance, the upregulations of peroxisome proliferator-activated receptor gamma (PPARγ) and leptin have been shown to stimulate angiogenesis [34,73]. Furthermore, it has been reported that the co-culture of HUVECs and

differentiated adipocytes showed a vasculature network organization supported by the upregulation of vascular endothelial growth factor (VEGF) and leptin secretion from the adipocytes [74]. Leptin also induces the proliferation of HUVECs for a more rapid networking which is engendered in response to an increased VEGF release from the HUVECs as well [75]. By modeling the maintenance of this cross-talk in our vascularized adipose drop tissues, we could reproduce the BMI-dependent leptin regulation which was found to be lower, following the increase in obesity phenotype in the mature adipocytes.

Finally, to compare our model with other published models, only a few studies have directly used mature adipocytes seeding *in vitro*. Harms et al. [22] seeded human mature adipocytes packed below a transwell, which could maintain good functionality for up to 2 weeks of *in vitro* culture. However, the method itself is not convenient as each measurement requires the detachment of the mature adipocytes from the transwell, inducing a possible loss of cells during the assays and thus limiting its application to HTS. Another limitation is the lack of ECM surrounding the mature adipocytes, possibly impairing the full physiological functionality of the adipocytes. The model from Rogal et al. [25] kept human mature adipocytes encapsulated in a collagen gel in a chip with flow bringing nutrients and also reagents for performing the assays. They could maintain mature adipocytes for up to 36 days of culture, with associated fatty acids uptake or glycerol release, even if lower functionality was found after the 36 days. This on-a-chip model appeared to be more suitable for HTS application. Lau et al. also added ECM to their model, in the form of gelatin gel, less similar than the *in vivo* collagen, to construct a sandwiched model with mature adipocytes encapsulated between two layers of ADSC-embedded gelatin gels [26]. It allowed the maintenance of mature adipocytes viability for up to 3 weeks, but leptin secretion as well as glycerol release were only possible for up to 5 days of culture. Also, its HTS application is limited due to the low number of tissues that can be assessed at the same time. While these models did show valuable improvements compared to the previous 2D models or even the differentiated preadipocyte models, none of them considered the specific BMI ranges phenotype that mature adipocytes exhibit in cases of obesity.

4. Conclusion

This developped model of vascularized and non-vascularized adipose drop tissues should be compatible with high throughput formats for adipose-targeting drug screening, displaying a wide range of measurable functional outputs like viability, hormone secretion, lipogenesis, lipolysis or glycerol secretion, in a robust and responsive model. Moreover, it was validated by the current quality control metrics, Z′-factor, S/N, S/B, CV, SSMD and CVD, as a robust model for HTS applications. To address this possibility, the handling of the 96-well plates could possibly be used in automated device methodologies such as robotic liquid handling and high-content imaging assays for addressing the needs of pharmaceuticals companies.

Another application can also be for personalized medical applications where cells from a specific patient's adipose tissue can be isolated and seeded to obtain accurate data about the possible drugs that can be used specifically for that patient. Additionally, knowing that adipose tissue expansion could be controlled through angiogenesis prevention [34,76], the vascularized adipose drop tissues could also be of interest for the development of new experimental obesity treatments targeting the blood vessels vasculature.

For the future approach, the addition of adipose macrophages in the vascularized drops tissue model should hold promises for a better understanding of their association between the blood vessels and adipocytes, being linked to the inflammatory responses observed in a broad range of obesity-associated diseases, like in diet-induced type 2 diabetes and insulin resistance [77,78].

5. Experimental section/methods

Materials: Porcine type I collagen were kindly donated from Nippon Ham (Osaka, Japan). Fibrinogen (from bovine plasma, F8630), Thrombin (from bovine plasma, T4648), Glycerol Assay Kit (MAK117), Bovine serum albumin (BSA, A3294), Human Adipocyte Differentiation Medium (Cell Applications, 811D-250), Insulin from bovine pancreas (I6634), Cytochalasin B from Drechslera dematioidea Solution (C2743), all-TRANS retinoic acid (R2625), Forskolin (F3917), Rosiglitazone (R2408), Phosphate buffered saline powder (PBS, D5652), Collagenase from *Clostridium histolyticum* (Type I, C0130) and Triton-X 100 (T8787) were purchased from Sigma-Aldrich (St Louis, MO, USA). Fetal bovine serum (35010CV) was purchased from Corning (Corning, NY, USA). Penicillin, streptomycin, Nile Red (N1142), Human Leptin Quantikine ELISA Kit (DLP00, R&D systems), BODIPY™ 500/510 C1, C12 (4,4-Difluoro-5-Methyl-4-Bora-3a,4a-Diaza-s-Indacene-3-Dodecanoic Acid, (D3823)), goat anti-mouse secondary antibody Alexa Fluor® 647, Live/Dead® viability assay kit (Molecular Probes®, L3224) and Hoechst 33324 (H3570) were obtained from Thermo Fisher Scientific (Whaltam, MA, USA). 4%-paraformaldehyde (16310245) and Tumor Necrosis Factor-α (TNF-α, 94948-59-1) came from Wako Pure Chemical Industries (Tokyo, Japan). Mouse anti-human CD31 antibody (M0823) and mouse anti-human Collagen type IV antibody (M0785) were purchased from Dako Denmark A/S (Glostrup, Denmark). Mouse anti-human Laminin antibody (NCL-LAM-89) was obtained from Leica Biosystems (Newcastle, UK). Human umbilical vein endothelial cell (HUVEC, C25271) and endothelial growth medium (EGM-2MV, CC4147) were purchased from LONZA (Basel, Switzerland). Dulbecco's Modified Eagle Medium (DMEM) came from Nacalai Tesque Inc. (Kyoto, Japan). Glucose Uptake Cell-Based Assay Kit (600470) was bought from Cayman Chemicals (Ann Arbor, MI, United States).

Collagen microfibers preparation: Based on our previous studies [45,46,79–81], the collagen microfibers (CMF) were first prepared from a collagen type I sponge after dehydration condensation at 200 °C for 24 h crosslinking. The crosslinked collagen sponge was mixed with ultra-pure water at a concentration of 10 mg/mL (pH = 7.4, 25 °C) and homogenized for 6 min at 30 000 rpm (Violamo VH-10 homogenizer, S10N-10G diameter of 10 mm and 115 mm length). Then, the solution was ultrasonicated (Ultrasonic processor VC50, 50W, 20 kHz) in an ice bath for 100 cycles (1 cycle comprised 20 s ultrasonication and 10 s cooling) and filtrated (40 μm filter, microsyringe 25 mm filter holder, Merck), before being freeze-dried for 48 h (Freeze dryer FDU-2200, Eyela Co.). The obtained CMF was kept in a desiccator at room temperature.

Isolation of mature adipocytes and ADSC from adipose tissues: Abdominal human adipose tissues from patients were isolated at the Kyoto Prefectural University of Medicine Hospital and kept on an ice pack during the transportation until Osaka University (for Fig. 2h, thigh adipose tissue and breast adipose tissue were also used). The tissues were first washed in PBS containing 5% of antibiotics. Then, 8-10 g of tissue were separated into fragments to fill the 6 wells of a 6-well plate and were minced to get around 1 mm^3 in size using autoclaved scissors and tweeters, directly in 2 mL of collagenase solution at 2 mg/mL in DMEM 0% FBS, 5% BSA and 1% antibiotics (sterilized by filtration). After 1 h of incubation at 37 °C with 250 rpm rotation, DMEM medium was added and the lysate was filtrated using a sterilized 500 μm iron mesh filter, before being centrifuged 3 min at 80g. After centrifugation, mature adipocytes were found at the top layer, while stromal vascular fraction containing ADSC and blood cells were in the pellet. The liquid between the top layer and the pellet was thus aspirated and discarded using a long needle and a 10 mL syringe between each wash. The cells were washed two times in PBS with 5% BSA and 1% antibiotics and once in complete DMEM, by 3 min of centrifugation at 80*g* between each wash. Then, the pellet was resuspended in DMEM for ADSC expansion by changing the medium every day during three days and then passage the cells when they reach 80% of confluency. The mature adipocytes layer was moved to a new tube and cells were counted staining the nuclei

during 15 min with Hoechst in DMEM and using a Turker Burk hematocytometer on a fluorescent microscope.

Cell culture in the CMF drops tissues and in 2D condition: To construct the fat tissues, collagen microfibers (CMF) were first weighted and washed in DMEM without FBS before being centrifuged 1 min at 10 000 rpm to get a final concentration in the tissues of 1.2%wt (Minispin, ThermoFisher Scientific, Whaltam, MA, USA). When needed, the ADSC and the HUVEC were added after trypsin detachment (always used at passages 1-5) and centrifuged 1 min at 3500 rpm (Minispin, ThermoFisher Scientific, Whaltam, MA, USA) to get a final cell concentration of 3×10^6 ADSC/mL and 1.5×10^6 HUVEC/mL. The pellet containing CMF, ADSC and HUVEC was then mixed with the fibrinogen solution (to get a final concentration at 6 mg/mL, stock solution in DMEM 0% FBS 1% antibiotics, filtrated using a 0.2 μm filter) and the thrombin solution (to get a final concentration of 3U/mL, stock solution in DMEM 10% FBS 1% antibiotics, filtrated using a 0.2 μm filter). Finally, the mature adipocytes were added at a final concentration of 3.5×10^6 cells/mL and the tissues were directly seeded in the 96 well plate (Iwaki, 3860-096, Yoshida, Japan) (see Fig. 1). The gelation occured during 15 min in the incubator at 37 °C, then 300 μL of medium were added. DMEM was used for the adipose tissues or EGM-2 medium +10 μg/mL of final concentration of insulin for the vascularized adipose tissues. The culture medium was renewed every 2-3 days.

For the preliminary developments, 4 different seeding conditions were compared, with different CMF concentrations, cells concentrations and medium volumes. Condition 1: 3.5×10^6 mature adipocytes/mL + 2.4%wt CMF, condition 2: 3.5×10^6 mature adipocytes/mL + 1.2%wt CMF, condition 3: 1.75×10^6 mature adipocytes/mL + 1.2%wt CMF, condition 4: 3.5×10^6 mature adipocytes/mL + 0%wt CMF) and the culture medium volume (96 well: 300 μL, 48 well: 1.2 mL). Then, using the condition 2 mixture, different drops volumes seeding were compared: 1, 2, 3 and 5 μL in 96 well plates.

For the ADSC culture, 10^6 ADSC/mL with 1.2%wt CMF mixture condition was used in 3D and 18 000 ADSC was seeded in 2D in 96 well plates in 300 μL of DMEM medium. For adipogenic differentiation, three days of proliferation were necessary for reaching cells confluence in 2D or cell aggregates in 3D, medium was then switched for Human Adipocyte Differentiation Medium to induce the adipogenesis. The 300 μL of differentiation medium was then renewed every 2-3 days until 14 days of differentiation. Retinoic acid was also added in the Human Adipocytes Differentiation culture medium, from the differentiation step at 1, 5, 10 and 25 μM and renewed at each medium change.

Viability assessment: The viability of cells was quantified using the Live/Dead® viability assay kit. After one PBS wash, the tissues were stained (Green: live cells, red: dead cells) during 1 h at 37 °C in the dark and then imaged using epifluorescence Confocal Quantitative Image Cytometer CQ1 (Yokogawa, Tokyo, Japan). Z-stack with the same steps and using maximum intensity projection was performed keeping same exposition time and excitation power for each sample. ImageJ software (Fiji, version 1.52s) was used for the analysis of the projections, calculating the percentage of each staining.

Glucose and fatty acids uptakes measurements: Glucose starvation was first applied on the drop tissues by renewing the culture medium with 300 μL of DMEM without glucose, with 1% BSA and 1% antibiotics, after one PBS wash, and incubated during 6 h in the incubator at 37 °C. For the fatty acids uptake assessment, the inhibitor TNFα was also added during the starvation step. After the 6 h of starvation, the glucose (2-NBDG, 2-deoxy-2-((7-nitro-2,1,3-benzoxadiazol-4-yl)amino)-D-glucose from the Glucose uptake assay kit) and fatty acids (BODIPY™ 500/510) fluorescent analogues were prepared in the DMEM without glucose with 1% BSA and 1% antibiotics, at 0.1 mg/mL final concentration for the 2-NBDG and 4 μM final concentration for the BODIPY, following the manufacturers protocols. In the mixture, inducers and activators were also added at a final concentration of: Insulin 20 μg/mL, Cytochalasin B 50 μM, Apigenin 250 μM (from the Glucose uptake assay kit) and TNFα 100 ng/mL, for a volume of 100 μL per well. After 5 min, the DMEM without glucose medium containing the 2-NBDG or the BODIPY with their activators/inhibitors was moved to an eppendorf tube and the adipose drop tissues were washed twice with 300 μL of warm PBS. The fluorescence intensity in a new 300 μL of PBS was then measured using a plate reader at 488 nm (Synergy HTX Plate Reader, BioTek Instruments Inc., Winooski, VT, USA), on the drop tissue location at the bottom and the middle of each well. Different gains were used for the measurement, according to 2-NBDG or BODIPY because their fluorescence intensities were different (2-NBDG gain: 39, BODIPY gain: 65), both gains were determined during the first experiment and were kept the same for all the experiments to be able to compare the results. Pictures of fluorescent glucose and fatty acids analogues uptakes were performed using an epifluorescence microscope (Confocal Quantitative Image Cytometer CQ1, Tokyo, Yokogawa). The supernatant PBS was then aspirated and the DMEM without glucose medium containing the 2-NBDG or the BODIPY with their activators/inhibitors was put back in the well containing the adipose drop tissues for additional 25 min to get the value of the glucose uptake/fatty acids uptake after 30 min, as well as additional 30 min to get the 60 min values. Before each measurement and pictures, the medium was removed and kept for later use, then washed three times with PBS for the measurement.

For the ADSC cultures conditions, the 2D monolayer of cells detached easily from the well surface so it was impossible to perform several washes at 5, 30 and 60 min to measure the glucose and fatty acids uptakes or cells were lost after each measure. It was thus decided to perform only the last measurement at 60 min of incubation, keeping for this measure the 3 x PBS washes before, on the 3D and 2D conditions. Pictures were also performed using an epifluorescence microscope (Confocal Quantitative Image Cytometer CQ1, Tokyo, Yokogawa).

For the quantifications, the fluorescence intensities were measured on drops or 2D conditions first in PBS without adding the glucose and fatty acids analogues. This value represents the 0% at 0 min. Then all data were represented in percentages compared to this 0 value. Fig. 3g and h and the Supplementary Figure 3 representing the average of the data for the 9-18 different patients were expressed compared to the control condition (without insulin or inhibitors) of each patient at 5 min for the 0%. In Fig. 5a–c, the insulin sensitivity is expressed by the value for each patient of the glucose uptake increase ratio compared to the control after 30 min of insulin incubation (1 represent insulin resistance with no insulin response observed).

Glycerol release measurements: For the glucose releases, the supernatant was aspirated and the adipose drops were washed twice with PBS. Then, 100 μL of new DMEM without glucose, with 1% BSA and 1% antibiotics was added with additional Insulin 20 μg/mL (inhibitor), Forskolin 100 and 200 μM (inducer) or Isoproterenol 2 mM (inducer), during 60 min. Finally, 10 μL of the supernatant was taken for the glycerol release assay, following the manufacturer protocol and using a plate reader (Synergy HTX Plate Reader, BioTek Instruments Inc., Winooski, VT, USA) for the samples and the standard curve colorimetric measurement of the absorbance at 570 nm.

Rosiglitazone and Melatonin treatments: 16 h before the assay, Rosiglitazone and Melatonin were added in the culture medium (DMEM) at final concentrations of 0, 0.1, 1, 10, 20 and 50 μM for the Rosiglitazone and 0, 0.1, 1 and 10 μM for the Melatonin. The Rosiglitazone and Melatonin were kept in the mixture even during the glucose uptake measurement, whose method was already described above.

Leptin Enzyme-linked immunosorbent assays: Culture media conditioned for 2 days were harvested from the supernatant of the adipose drops each week during 3 weeks. Supernatant were then centrifuged at 15,000 g for 5 min, and stored at −80 °C until analysis. Secreted leptin levels were expressed as pg/ml of medium, following the manufacturer's protocol.

Immunofluorescence imaging: Tissues were fixed with 4% paraformaldehyde solution in PBS overnight at 4 °C. Samples were permeabilized in 0.05% Triton X-100 in PBS for 7 min and incubated 1 h at room temperature in 1% BSA in PBS to minimize non-specific staining.

Anti-CD31 antibody was added in BSA 1% and incubated overnight at 4 °C. Finally, samples were incubated with Secondary Antibodies Alexa Fluor® 647, at room temperature in the dark for 2 h. Nuclei were counterstained with Hoechst. The samples were rinsed in PBS and observed using an epifluorescence microscope (Confocal Quantitative Image Cytometer CQ1, Tokyo, Yokogawa). Intracellular lipid accumulation was stained using Nile Red™ compound diluted in PBS, with nuclei counterstained by Hoechst.

Lipid and DNA content assay: The Orr et al.'s method [82] was followed with slight differences. Briefly, 20-25 mg of tissue coming from abdominal human adipose tissues (3 different patients) or 3 independent seeded vascularized adipose drops tissues experiments (3 different patients, 10 drops per experiment) were completely homogenized in 1 mL PBS by using sequential gauges needles with 1 mL syringe (15G, 19G, 21G and then 27G). Then, 100 μL of each lysate was added in black 96 well microplate and mixed with 100 μL of 25 μg/mL of Nile Red solution prepared in DMSO. After 10 min of incubation at 37 °C, the plate was agitated and the fluorescence was measured (Ex. 540, Em. 590) with a plate reader (Synergy HTX Plate Reader, BioTek Instruments Inc., Winooski, VT, USA). To validate the method, a standard curve was performed in parallel using Oleic acid (O1383, Sigma Aldrich) (Supplementary Figure 1). In separated wells, 100 μL of each lysate in PBS was again added in the 96 well plate, mixed only with 1 μL of Hoechst to also evaluate the DNA fluorescence after 10 min of incubation (Ex. 360/Em. 460) as normalization, additionally to the tissues wet weight measured before the lysis.

For the quantitative measurement of the DNA, other samples and drops tissues from the same patients were added in 200 μL of ATL lysis buffer with Proteinase K (DNeasy Blood & Tissue Kit, 69504, QIAGEN, Hilden, Germany) and after 1 h of lysis at 56 °C, the Qubit™ dsDNA BR Assay Kit (Thermo Fisher Scientific MA, USA) was used to quantify the DNA concentration, following the protocol guidelines with the Qubit fluorometer. The DNA amount was then normalized by the tissues wet weight measured before lysis.

Ethics statement: The adipose tissues were collected from Kyoto Prefectural University of Medicine Hospital (Kyoto, Japan) after abdominal adipose tissues, breast adipose tissues or liposuction isolation of different human female donors at the ages between 35 and 72 years old, and BMI between 14.2 and 36.6. All use was approved by the Human Ethics Committee (Approval number: ERB-C-1317-1) of the Kyoto Prefectural University of Medicine Institutional Review Board and conformed to the principles outlined in the Declaration of Helsinki.

Statistical analysis: Statistical analyses were performed using EzAnova software (version 0.98) by Tukey multiple comparison test (double-way ANOVA). For data that compared only one factor, one-way ANOVA was performed if the number of measures was the same, otherwise T Student test was performed. Error bars represent SD. p values were considered significantly different at least when $p < 0.05$ and were represented as: * is $p < 0.05$, ** is $p < 0.01$ and *** is $p < 0.001$. When no marks are shown on the graphs, it means that the differences are not significant.

For the HTS validation statistics, different screening assay quality parameters were calculated after using the commonly used log-transformation on the data [70,72]. For this analysis, mature adipocytes from a healthy patient (BMI 24.5, 49 years old) seeded in monoculture drops at day 0 (the day of seeding) were used, providing a negative control being the T_0 (no glucose or fatty acids uptakes) and a positive control being the $T_{30\ min}$ of the glucose and fatty acids uptakes following insulin treatment after 6h of glucose starvation, as explained already above. This positive control condition was used for the fluorescence linearity assessment as well, but with varying cell number.

The following parameters were assessed [69,72]:

- The assay quality metric Z', which was introduced in 1999 by Zhang et al.

$$1 - \frac{3*(\sigma_{pc} + \sigma_{nc})}{|\mu_{pc} - \mu_{nc}|}$$

where σ and μ are the standard deviation and mean, respectively of the normalized positive (pc) and negative control (nc) populations, considering not only the amplitude of responses but also their variance.

- The Signal-to-Noise (S/N) and Signal-to-Background (S/B) ratios

$$S/N = \frac{\mu_{pc} - \mu_{nc}}{\sigma_{nc}} \text{ and } S/B = \frac{\mu_{pc}}{\mu_{nc}}$$

- The coefficients of variation (CV) associated with the measurement technique, which are standardized measures for the dispersion of a distribution

$$CV_{max}\ (\%) = \frac{\sigma_{pc}}{\mu_{pc}} \times 100$$

$$CV_{min}\ (\%) = \frac{\sigma_{nc}}{\mu_{nc}} \times 100$$

- The strictly standardized mean difference (SSMD) and its reciprocal, the coefficient of variation of difference (CVD), for measuring the magnitude of difference between two populations

$$SSMD = \frac{\mu_{pc} - \mu_{nc}}{\sqrt{{\sigma_{pc}}^2 + {\sigma_{nc}}^2}}$$

$$CVD = \frac{\sqrt{{\sigma_{pc}}^2 + {\sigma_{nc}}^2}}{\mu_{pc} - \mu_{nc}}$$

- The assessment of fluorescence linearity: In a separate experiment, the same mature adipocytes were seeded in drops tissues after being diluted serially. 8 replicate wells for each cell number were then also analyzed for their glucose and fatty acids uptake after 30 min of insulin induction. Fluorescence was measured and the background fluorescence for the empty wells, as well as the drop tissues without 2-NBDG or BODIPY background were subtracted, and the fluorescence was then plotted and analyzed by linear regression.

Data availability

The data that support the findings of this study are available from the corresponding author, MM, upon reasonable request.

CRediT authorship contribution statement

Fiona Louis: Conceptualization, Methodology, Validation, Formal analysis, Investigation, Resources, Visualization, Writing – original draft, Writing – review & editing, Funding acquisition. **Yoshihiro Sowa:** Conceptualization, Methodology, Validation, Investigation, Resources, Visualization, Writing – original draft, Writing – review & editing, Supervision, Funding acquisition. **Shiro Kitano:** Resources, Writing – review & editing, Supervision, Project administration. **Michiya Matsusaki:** Conceptualization, Methodology, Resources, Writing – review & editing, Supervision, Project administration.

Declaration of competing interests

The authors declare that they have no known competing financial interests or personal relationships that could have appeared to influence the work reported in this paper.

Acknowledgements

The authors thank Nippon Ham Foods Ltd for their kind donation of collagen. This research was supported by a Kakenhi Grant-in-Aid for Early-Career Scientists (70838523), as well as a grant from the Japanese Ministry of Education, Culture, Sports, Science and Technology (18K09488).

Appendix A. Supplementary data

Supplementary data to this article can be found online at https://doi.org/10.1016/j.bioactmat.2021.05.020.

References

[1] Obesity and overweight, (n.d.). https://www.who.int/news-room/fact-sheets/detail/obesity-and-overweight (accessed May 7, 2020).
[2] IDF Diabetes Atlas, (n.d.). https://www.idf.org/e-library/epidemiology-research/diabetes-atlas/159-idf-diabetes-atlas-ninth-edition-2019.html (accessed May 7, 2020).
[3] N.J. Switzer, H.S. Mangat, S. Karmali, Current trends in obesity: body composition assessment, weight regulation, and emerging techniques in managing severe obesity, J. Intervent. Gastroenterol. 3 (2013) 34–36.
[4] M.A. van Baak, Nutrition as a link between obesity and cardiovascular disease: how can we stop the obesity epidemic? Thromb. Haemostasis 110 (2013) 689–696, https://doi.org/10.1160/TH13-01-0045.
[5] P. Gu, A. Xu, Interplay between adipose tissue and blood vessels in obesity and vascular dysfunction, Rev. Endocr. Metab. Disord. 14 (2013) 49–58, https://doi.org/10.1007/s11154-012-9230-8.
[6] E.D. Rosen, B.M. Spiegelman, What we talk about when we talk about fat, Cell 156 (2014) 20–44, https://doi.org/10.1016/j.cell.2013.12.012.
[7] L. Casteilla, L. Pénicaud, B. Cousin, D. Calise, Choosing an adipose tissue depot for sampling, in: K. Yang (Ed.), Adipose Tissue Protocols, Humana Press, Totowa, NJ, 2008, pp. 23–38, https://doi.org/10.1007/978-1-59745-245-8_2.
[8] D.E. Chusyd, D. Wang, D.M. Huffman, T.R. Nagy, Relationships between rodent white adipose fat pads and human white adipose fat depots, Front. Nutr. 3 (2016), https://doi.org/10.3389/fnut.2016.00010.
[9] S. Cinti, The role of brown adipose tissue in human obesity, Nutr. Metabol. Cardiovasc. Dis. 16 (2006) 569–574, https://doi.org/10.1016/j.numecd.2006.07.009.
[10] J.P. Hughes, S. Rees, S.B. Kalindjian, K.L. Philpott, Principles of early drug discovery, Br. J. Pharmacol. 162 (2011) 1239–1249.
[11] F. Louis, M. Matsusaki, 15 - adipose tissue engineering, in: N.E. Vrana, H. Knopf-Marques, J. Barthes (Eds.), Biomaterials for Organ and Tissue Regeneration, Woodhead Publishing, 2020, pp. 393–423, https://doi.org/10.1016/B978-0-08-102906-0.00008-8.
[12] X. Wang, L. Gao, Y. Han, M. Xing, C. Zhao, J. Peng, J. Chang, Silicon-enhanced adipogenesis and angiogenesis for vascularized adipose tissue engineering, Adv. Sci. 5 (2018), https://doi.org/10.1002/advs.201800776.
[13] O. Huttala, M. Palmroth, P. Hemminki, T. Toimela, T. Heinonen, T. Ylikomi, J.-R. Sarkanen, Development of versatile human in vitro vascularized adipose tissue model with serum-free angiogenesis and natural adipogenesis induction, Basic Clin. Pharmacol. Toxicol. (2018), https://doi.org/10.1111/bcpt.12987, 0.
[14] S. Gogg, A. Nerstedt, J. Boren, U. Smith, Human adipose tissue microvascular endothelial cells secrete PPARγ ligands and regulate adipose tissue lipid uptake, JCI Insight 4 (2019), https://doi.org/10.1172/jci.insight.125914.
[15] K. Duval, H. Grover, L.-H. Han, Y. Mou, A.F. Pegoraro, J. Fredberg, Z. Chen, Modeling physiological events in 2D vs. 3D cell culture, Physiology 32 (2017) 266–277, https://doi.org/10.1152/physiol.00036.2016.
[16] M. Ravi, V. Paramesh, S.R. Kaviya, E. Anuradha, F.D.P. Solomon, 3D cell culture systems: advantages and applications, J. Cell. Physiol. 230 (2015) 16–26, https://doi.org/10.1002/jcp.24683.
[17] S.A. Langhans, Three-Dimensional in vitro cell culture models in drug discovery and drug repositioning, Front. Pharmacol. 9 (2018), https://doi.org/10.3389/fphar.2018.00006.
[18] A. Saiki, F. Watanabe, T. Murano, Y. Miyashita, K. Shirai, Hepatocyte growth factor secreted by cultured adipocytes promotes tube formation of vascular endothelial cells in vitro, Int. J. Obes. 30 (2006) 1676–1684, https://doi.org/10.1038/sj.ijo.0803316.
[19] S. Aoki, S. Toda, T. Sakemi, H. Sugihara, Coculture of endothelial cells and mature adipocytes actively promotes immature preadipocyte development in vitro, Cell Struct. Funct. 28 (2003) 55–60, https://doi.org/10.1247/csf.28.55.
[20] P.A. Zuk, M. Zhu, P. Ashjian, D.A. De Ugarte, J.I. Huang, H. Mizuno, Z.C. Alfonso, J.K. Fraser, P. Benhaim, M.H. Hedrick, Human adipose tissue is a source of multipotent stem cells, Mol. Biol. Cell 13 (2002) 4279–4295, https://doi.org/10.1091/mbc.E02-02-0105.
[21] A.-C. Volz, B. Omengo, S. Gehrke, P.J. Kluger, Comparing the Use of Differentiated Adipose-Derived Stem Cells and Mature Adipocytes to Model Adipose Tissue in Vitro, 2019, https://doi.org/10.1016/j.diff.2019.09.002. Differentiation.
[22] M.J. Harms, Q. Li, S. Lee, C. Zhang, B. Kull, S. Hallen, A. Thorell, I. Alexandersson, C.E. Hagberg, X.-R. Peng, A. Mardinoglu, K.L. Spalding, J. Boucher, Mature human white adipocytes cultured under membranes maintain identity, function, and can transdifferentiate into Brown-like adipocytes, Cell Rep. 27 (2019) 213–225, https://doi.org/10.1016/j.celrep.2019.03.026, e5.
[23] B. Huber, K. Borchers, G.E. Tovar, P.J. Kluger, Methacrylated gelatin and mature adipocytes are promising components for adipose tissue engineering, J. Biomater. Appl. 30 (2016) 699–710, https://doi.org/10.1177/0885328215587450.
[24] S. Toda, K. Uchihashi, S. Aoki, E. Sonoda, F. Yamasaki, M. Piao, A. Ootani, N. Yonemitsu, H. Sugihara, Adipose tissue-organotypic culture system as a promising model for studying adipose tissue biology and regeneration, Organogenesis 5 (2009) 50–56.
[25] J. Rogal, C. Binder, E. Kromidas, J. Roosz, C. Probst, S. Schneider, K. Schenke-Layland, P. Loskill, WAT-on-a-chip integrating human mature white adipocytes for mechanistic research and pharmaceutical applications, Sci. Rep. 10 (2020) 1–12, https://doi.org/10.1038/s41598-020-63710-4.
[26] F.H. Lau, K. Vogel, J.P. Luckett, M. Hunt, A. Meyer, C.L. Rogers, O. Tessler, C. L. Dupin, H. St Hilaire, K.N. Islam, T. Frazier, J.M. Gimble, S. Scahill, Sandwiched white adipose tissue: a microphysiological system of primary human adipose tissue, tissue engineering Part C, Methods 24 (2017) 135–145, https://doi.org/10.1089/ten.tec.2017.0339.
[27] U. Smith, B.B. Kahn, Adipose tissue regulates insulin sensitivity: role of adipogenesis, de novo lipogenesis and novel lipids, J. Intern. Med. 280 (2016) 465–475, https://doi.org/10.1111/joim.12540.
[28] D. Antoni, H. Burckel, E. Josset, G. Noel, Three-Dimensional cell culture: a breakthrough in vivo, Int. J. Mol. Sci. 16 (2015) 5517–5527, https://doi.org/10.3390/ijms16035517.
[29] A. Gastaldelli, M. Gaggini, R.A. DeFronzo, Role of adipose tissue insulin resistance in the natural history of type 2 diabetes: results from the san antonio metabolism study, Diabetes 66 (2017) 815–822, https://doi.org/10.2337/db16-1167.
[30] S.-L. Ryan, A.-M. Baird, G. Vaz, A.J. Urquhart, hias Senge, D.J. Richard, K. J. O'Byrne, A.M. Davies, Drug discovery approaches utilizing three-dimensional cell culture, Assay Drug Dev. Technol. 14 (2016) 19–28, https://doi.org/10.1089/adt.2015.670.
[31] P. Kongsuphol, S. Gupta, Y. Liu, S.B.N. Gourikutty, S.K. Biswas, Q. Ramadan, In vitro micro-physiological model of the inflamed human adipose tissue for immune-metabolic analysis in type II diabetes, Sci. Rep. 9 (2019) 1–14, https://doi.org/10.1038/s41598-019-41338-3.
[32] S.B. Park, B. Koh, W.H. Jung, K.J. Choi, Y.J. Na, H.M. Yoo, S. Lee, D. Kang, D.-M. Lee, K.Y. Kim, Development of a three-dimensional in vitro co-culture model to increase drug selectivity for humans, Diabetes Obes. Metabol. (2020), https://doi.org/10.1111/dom.14033.
[33] J. Rogal, A. Zbinden, K. Schenke-Layland, P. Loskill, Stem-cell based organ-on-a-chip models for diabetes research, Adv. Drug Deliv. Rev. 140 (2019) 101–128, https://doi.org/10.1016/j.addr.2018.10.010.
[34] Y. Cao, Angiogenesis and vascular functions in modulation of obesity, adipose metabolism, and insulin sensitivity, Cell Metabol. 18 (2013) 478–489, https://doi.org/10.1016/j.cmet.2013.08.008.
[35] J. Borges, M.C. Müller, A. Momeni, G.B. Stark, N. Torio-Padron, In vitro analysis of the interactions between preadipocytes and endothelial cells in a 3D fibrin matrix, Minim Invasive Ther. Allied Technol. 16 (2007) 141–148, https://doi.org/10.1080/13645700600935398.
[36] D.O. Traktuev, D.N. Prater, S. Merfeld-Clauss, A.R. Sanjeevaiah, M.R. Saadatzadeh, M. Murphy, B.H. Johnstone, D.A. Ingram, K.L. March, Robust functional vascular network formation in vivo by cooperation of adipose progenitor and endothelial cells, Circ, Res. 104 (2009) 1410–1420, https://doi.org/10.1161/CIRCRESAHA.108.190926.
[37] E. Bellas, K.G. Marra, D.L. Kaplan, Sustainable three-dimensional tissue model of human adipose tissue, Tissue Eng. C Methods 19 (2013) 745–754, https://doi.org/10.1089/ten.TEC.2012.0620.
[38] X. Cai, J. Xie, Y. Yao, X. Cun, S. Lin, T. Tian, B. Zhu, Y. Lin, Angiogenesis in a 3D model containing adipose tissue stem cells and endothelial cells is mediated by canonical Wnt signaling, Bone Research 5 (2017) 1–13.
[39] J.H. Kang, J.M. Gimble, D.L. Kaplan, In vitro 3D model for human vascularized adipose tissue, Tissue Eng Part A 15 (2009) 2227–2236, https://doi.org/10.1089/ten.tea.2008.0469.
[40] K. Aubin, M. Safoine, M. Proulx, M.-A. Audet-Casgrain, J.-F. Côté, F.-A. Têtu, A. Roy, J. Fradette, Characterization of in vitro engineered human adipose tissues: relevant adipokine secretion and impact of TNF-α, PloS One 10 (2015) https://doi.org/10.1371/journal.pone.0137612 e0137612.
[41] O. Huttala, J.-R. Sarkanen, T. Heinonen, T. Ylikomi, in: Presence of Vasculature Results in Faster Insulin Response in Adipocytes in Vascularized Adipose Tissue Model, vol. 1, 2019, pp. 419–434, https://doi.org/10.14573/altex.1811271, 36.
[42] A.-C. Volz, L. Hack, F.B. Atzinger, P.J. Kluger, Completely defined co-culture of adipogenic differentiated ASCs and microvascular endothelial cells, ALTEX 35 (2018) 464–476, https://doi.org/10.14573/altex.1802191.
[43] A.-C. Volz, B. Huber, P.J. Kluger, Adipose-derived stem cell differentiation as a basic tool for vascularized adipose tissue engineering, Differentiation 92 (2016) 52–64, https://doi.org/10.1016/j.diff.2016.02.003.
[44] L. Benmeridja, L. De Moor, E. De Maere, F. Vanlauwe, M. Ryx, L. Tytgat, C. Vercruysse, P. Dubruel, S. Van Vlierberghe, P. Blondeel, H. Declercq, High-throughput fabrication of vascularized adipose microtissues for 3D bioprinting, J Tissue Eng Regen Med (2020), https://doi.org/10.1002/term.3051.
[45] F. Louis, S. Kitano, J.F. Mano, M. Matsusaki, 3D collagen microfibers stimulate the functionality of preadipocytes and maintain the phenotype of mature adipocytes for long term cultures, Acta Biomater. 84 (2019) 194–207, https://doi.org/10.1016/j.actbio.2018.11.048.

[46] H. Liu, S. Kitano, S. Irie, R. Levato, M. Matsusaki, Collagen microfibers induce blood capillary orientation and open vascular lumen, Advanced Biosystems 4 (2020), https://doi.org/10.1002/adbi.202000038, 2000038.
[47] F. Louis, Y. Sowa, S. Irie, S. Kitano, O. Mazda, M. Matsusaki, Injectable Prevascularized Mature Adipose Tissues (iPAT) to Achieve Long-Term Survival in Soft Tissues Regeneration, BioRxiv, 2020, p. 2020, https://doi.org/10.1101/2020.12.07.415455, 12.07.415455.
[48] S. Wei, W.G. Bergen, G.J. Hausman, L. Zan, M.V. Dodson, Cell culture purity issues and DFAT cells, Biochem. Biophys. Res. Commun. 433 (2013) 273–275, https://doi.org/10.1016/j.bbrc.2013.03.006.
[49] R.T. Watson, J.E. Pessin, GLUT4 translocation: the last 200 nanometers, Cell, Signal 19 (2007) 2209–2217, https://doi.org/10.1016/j.cellsig.2007.06.003.
[50] J.M. Rutkowski, J.H. Stern, P.E. Scherer, The cell biology of fat expansion, J. Cell Biol. 208 (2015) 501–512, https://doi.org/10.1083/jcb.201409063.
[51] M. Nomura, T. Takahashi, N. Nagata, K. Tsutsumi, S. Kobayashi, T. Akiba, K. Yokogawa, S. Moritani, K. Miyamoto, Inhibitory mechanisms of flavonoids on insulin-stimulated glucose uptake in MC3T3-G2/PA6 adipose cells, Biol. Pharm. Bull. 31 (2008) 1403–1409, https://doi.org/10.1248/bpb.31.1403.
[52] B. Hellwig, H.G. Joost, Differentiation of erythrocyte-(GLUT1), liver-(GLUT2), and adipocyte-type (GLUT4) glucose transporters by binding of the inhibitory ligands cytochalasin B, forskolin, dipyridamole, and isobutylmethylxanthine, Mol. Pharmacol. 40 (1991) 383–389.
[53] W.P. Cawthorn, J.K. Sethi, TNF-α and adipocyte biology, FEBS Lett. 582 (2008) 117–131, https://doi.org/10.1016/j.febslet.2007.11.051.
[54] M. Schweiger, T.O. Eichmann, U. Taschler, R. Zimmermann, R. Zechner, A. Lass, Measurement of lipolysis, Methods Enzymol. 538 (2014) 171–193, https://doi.org/10.1016/B978-0-12-800280-3.00010-4.
[55] M. Kolodziej, S. Strauss, A. Lazaridis, V. Bucan, J.W. Kuhbier, P.M. Vogt, S. Könneker, Influence of glucose and insulin in human adipogenic differentiation models with adipose-derived stem cells, Adipocyte 8 (2019) 254–264, https://doi.org/10.1080/21623945.2019.1636626.
[56] S. Palacios-Ortega, M. Varela-Guruceaga, J.A. Martínez, C. de Miguel, F.I. Milagro, Effects of high glucose on caveolin-1 and insulin signaling in 3T3-L1 adipocytes, Adipocyte 5 (2015) 65–80, https://doi.org/10.1080/21623945.2015.1122856.
[57] E. Rush, WHO. World Health Organization (WHO) Expert Consultation: appropriate body-mass index for Asian populations and its implications for policy and intervention strategies, Lancet 363 (2004) 157–163, https://doi.org/10.1016/s0140-6736(03)15268-3.
[58] J. Jih, A. Mukherjea, E. Vittinghoff, T.T. Nguyen, J.Y. Tsoh, Y. Fukuoka, M. S. Bender, W. Tseng, A.M. Kanaya, Using appropriate body mass index cut points for overweight and obesity among Asian Americans, Prev. Med. 65 (2014) 1–6, https://doi.org/10.1016/j.ypmed.2014.04.010.
[59] B. Ahmed, R. Sultana, M.W. Greene, Adipose tissue and insulin resistance in obese, Biomed. Pharmacother. 137 (2021) 111315, https://doi.org/10.1016/j.biopha.2021.111315.
[60] N. Pannacciulli, R. Vettor, G. Milan, M. Granzotto, A. Catucci, G. Federspil, P. De Giacomo, R. Giorgino, G. De Pergola, Anorexia nervosa is characterized by increased adiponectin plasma levels and reduced nonoxidative glucose metabolism, None 88 (2003) 1748–1752, https://doi.org/10.1210/jc.2002-021215.
[61] B.S.Q. Rodriguez, R. Correa, Rosiglitazone, StatPearls Publishing, 2020. https://www.ncbi.nlm.nih.gov/books/NBK544230/. (Accessed 25 March 2020).
[62] S. Matthaei, M. Stumvoll, M. Kellerer, H.-U. Häring, Pathophysiology and pharmacological treatment of insulin resistance, Endocr. Rev. 21 (2000) 585–618, https://doi.org/10.1210/edrv.21.6.0413.
[63] R.A. Savage, S. Basnet, J.-M.M. Miller, Melatonin, StatPearls Publishing, 2019. https://www.ncbi.nlm.nih.gov/books/NBK534823/. (Accessed 25 March 2020).
[64] I. Nakajima, H. Aso, T. Yamaguchi, K. Ozutsumi, Adipose tissue extracellular matrix: newly organized by adipocytes during differentiation, Differentiation 63 (1998) 193–200, https://doi.org/10.1111/j.1432-0436.1998.00193.x.
[65] E.C.M. Mariman, P. Wang, Adipocyte extracellular matrix composition, dynamics and role in obesity, Cell. Mol. Life Sci. 67 (2010) 1277–1292, https://doi.org/10.1007/s00018-010-0263-4.
[66] S.Y. Chun, J.O. Lim, E.H. Lee, M.-H. Han, Y.-S. Ha, J.N. Lee, B.S. Kim, M.J. Park, M. Yeo, B. Jung, T.G. Kwon, Preparation and characterization of human adipose tissue-derived extracellular matrix, growth factors, and stem cells: a concise review, Tissue Eng Regen Med 16 (2019) 385–393, https://doi.org/10.1007/s13770-019-00199-7.
[67] M.D. Klok, S. Jakobsdottir, M.L. Drent, The role of leptin and ghrelin in the regulation of food intake and body weight in humans: a review, Obes. Rev. 8 (2007) 21–34, https://doi.org/10.1111/j.1467-789X.2006.00270.x.
[68] S. Carter, A. Caron, D. Richard, F. Picard, Role of leptin resistance in the development of obesity in older patients, Clin. Interv. Aging 8 (2013) 829–844, https://doi.org/10.2147/CIA.S36367.
[69] null Zhang, null Chung, null Oldenburg, A simple statistical parameter for use in evaluation and validation of high throughput screening assays, J. Biomol. Screen 4 (1999) 67–73, https://doi.org/10.1177/108705719900400206.
[70] Y. Sui, Z. Wu, Alternative statistical parameter for high-throughput screening assay quality assessment, J. Biomol. Screen 12 (2007) 229–234, https://doi.org/10.1177/1087057106296498.
[71] B. Wang, A.M. Goodpaster, M.A. Kennedy, Coefficient of variation, signal-to-noise ratio, and effects of normalization in validation of biomarkers from NMR-based metabonomics studies, Chemometr. Intell. Lab. Syst. 128 (2013) 9–16, https://doi.org/10.1016/j.chemolab.2013.07.007.
[72] X.D. Zhang, A pair of new statistical parameters for quality control in RNA interference high-throughput screening assays, Genomics 89 (2007) 552–561, https://doi.org/10.1016/j.ygeno.2006.12.014.
[73] O. Gealekman, A. Burkart, M. Chouinard, S.M. Nicoloro, J. Straubhaar, S. Corvera, Enhanced angiogenesis in obesity and in response to PPARgamma activators through adipocyte VEGF and ANGPTL4 production, Am. J. Physiol. Endocrinol. Metab. 295 (2008) E1056–E1064, https://doi.org/10.1152/ajpendo.90345.2008.
[74] J.H. Hammel, E. Bellas, Endothelial cell crosstalk improves browning but hinders white adipocyte maturation in 3D engineered adipose tissue, Int Bio (Cam). 12 (2020) 81–89, https://doi.org/10.1093/intbio/zyaa006.
[75] H.Y. Park, H.M. Kwon, H.J. Lim, B.K. Hong, J.Y. Lee, B.E. Park, Y. Jang, S.Y. Cho, H.S. Kim, Potential role of leptin in angiogenesis: leptin induces endothelial cell proliferation and expression of matrix metalloproteinases in vivo and in vitro, Exp. Mol. Med. 33 (2001) 95–102, https://doi.org/10.1038/emm.2001.17.
[76] A.C. Daquinag, Y. Zhang, M.G. Kolonin, Vascular targeting of adipose tissue as an anti-obesity approach, Trends Pharmacol. Sci. 32 (2011) 300–307, https://doi.org/10.1016/j.tips.2011.01.004.
[77] C.N. Lumeng, Adipose tissue macrophages: a piece of the PAI of metabolic syndrome, Sci. Transl. Med. 2 (2010), https://doi.org/10.1126/scitranslmed.3000850, 20ps7-20ps7.
[78] V.D. Dahik, E. Frisdal, W. Le Goff, Rewiring of lipid metabolism in adipose tissue macrophages in obesity: impact on insulin resistance and type 2 diabetes, Int. J. Mol. Sci. 21 (2020), https://doi.org/10.3390/ijms21155505.
[79] M.A. Abdul Sisak, F. Louis, S. Hyeok Lee, Y.-T. Chang, M. Matsusaki, Fabrication of blood capillary models for live imaging microarray analysis, Micromachines 11 (2020) 727, https://doi.org/10.3390/mi11080727.
[80] Y. Naka, S. Kitano, S. Irie, M. Matsusaki, Wholly vascularized millimeter-sized engineered tissues by cell-sized microscaffolds, Materials Today Bio 6 (2020) 100054, https://doi.org/10.1016/j.mtbio.2020.100054.
[81] A. Figarol, Y. Naka, Y. Shigemoto-Mogami, T. Furihata, K. Sato, M. Matsusaki, In Vitro self-organized three-dimensional model of the blood-brain barrier microvasculature, Biomed. Mater. (2020), https://doi.org/10.1088/1748-605X/aba5f1.
[82] V. Orr, L. Rehmann, Improvement of the Nile Red fluorescence assay for determination of total lipid content in microalgae independent of chlorophyll content, J. Appl. Phycol. 27 (2015) 2181–2189, https://doi.org/10.1007/s10811-014-0481-5.